FRACTALCOMS

Exploring the limits of Fractal Electrodynamics for the future telecommunication technologies
IST-2001-33055

Task 4.3 Final Report

Deliverable reference:	**D19**
Contractual Date of Delivery to the EC:	**January 31, 2004**
Author(s):	**José M. González, Jordi Romeu, Eugenia Cabot and Juan R. Mosig**
Participant(s):	**UPC and EPFL**
Workpackage:	**WP4**
Security:	**Public**
Nature:	**Deliverable**
Version:	**1.0**
Date:	**15-12-2003**

Total number of pages: 56

Abstract:

A summary of the measuring techniques used to characterize pre-fractal devices is presented in this report. The fabrication and characterization of some prototypes used to assess the measuring technique is also presented.

Keyword list: antenna, fractal, Wheeler cap, efficiency, quality factor, Hilbert, Koch, meander

TABLE OF CONTENTS

RELATED WP AND TASKS (FROM THE PROJECT DESCRIPTION)

WP 4: Fractal devices development.
Task 4.3: Prototype construction and measurement.

Objective: A few prototypes will be constructed and measured in order to validate the simulations and check the technology limitations. It is foreseen to construct and validate at least the following:

a) Miniature antenna. A prototype of miniature antenna that in accordance to the outputs of tasks 2.1, 4.1, and 4.2 approaches the fundamental limit for small antennas.

b) Miniature resonator. A prototype of miniature resonator in planar technology as potential building block for filter design will be verified.

In addition, other prototypes will be constructed thorough the project if necessary for experimental verification of the computer model.

1 SUMMARY

1.1 Measurement of radiation efficiency and quality factor of fractal antennas: the Wheeler cap method

Several methods used to characterize the performance of electrically small antennas have been reviewed, in order to select the one that best fits to the needs of the project: accuracy and repeatability for the measurement of small pre-fractal antennas radiation efficiency and quality factor. The radiation pattern measurement is of secondary importance because pattern differences among small antennas are negligible.

The following techniques to measure radiation efficiency and Q factor of antennas has been reviewed by UPC partner:

- the Wheeler Cap method;
- the Directivity/Gain method (also called Pattern Integration);
- the Radiometric method;
- the Q method;
- the Random Field Measurement Technique.

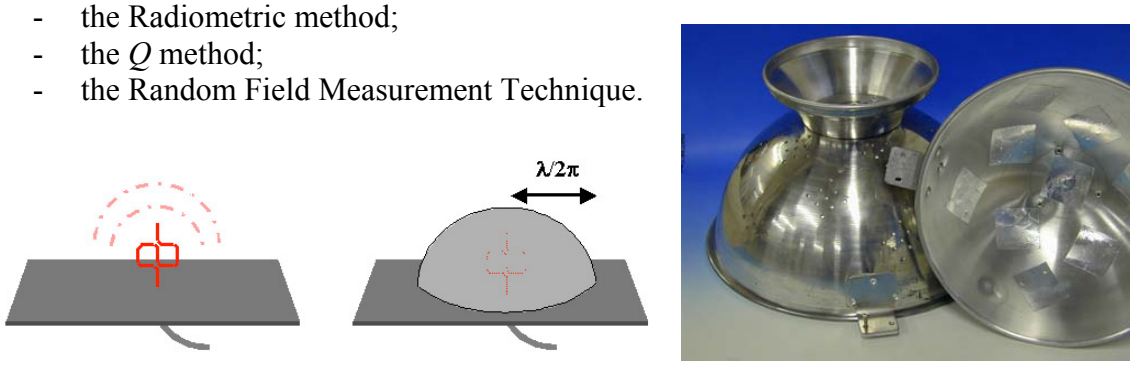

Figure I. Scheme of the Wheeler cap method and some of the Wheeler caps used in the measurements.

The Wheeler Cap method (Fig. I) has been implemented for the characterization of small pre-fractal antennas and conventional antennas. To assess the quality of the selected method in terms of accuracy, several experiments on well-known antennas have been carried out.

Through the development of the task:

- Experience has been gained on the design of small pre-fractal wire monopoles and its manufacturing using conventional printed circuits technology.
- Radiation shields as Wheeler caps have been designed for the most accurate measurement of radiation efficiency and quality factor.
- A post-processing technique has been developed in order to improve the accuracy of the measurement results.

1.2 Genetically designed planar monopoles

Genetically optimised planar monopoles have been designed in Task 4.1 to assess if fractal shapes are the best alternative for the design of efficient antennas with minimum resonant frequency. Koch-like, meander-line and zigzag monopoles have been analysed in the frame of this work. It was observed that Koch-like designs offer worst radiation performances than optimised meander-line and zigzag designs. Only in a few cases the pre-fractal designs attain similar performances than the Euclidean ones.

An example of these particular cases is shown in this section. A Koch-like optimum design was manufactured with the standard technique used for the fabrication of printed circuit boards, and compared with optimum meander-line and zigzag monopoles that with the same wire length yield have similar performance in the numerical simulations (Fig. II).

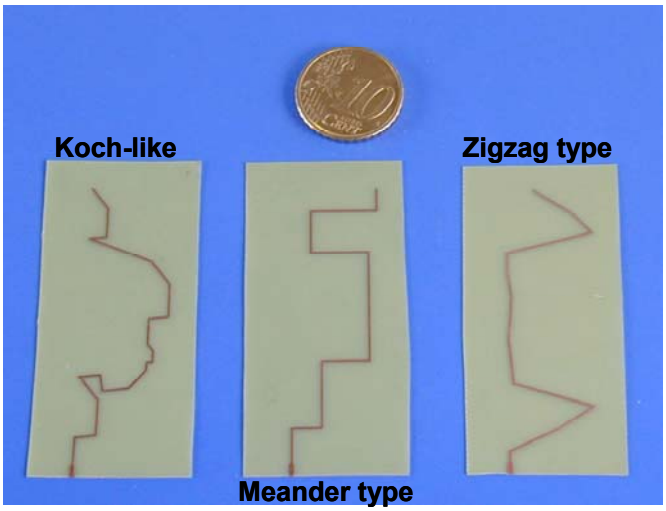

Figure II. Prototypes of genetically designed monopoles.

All these antennas were experimentally characterized using the Wheeler cap method. The experimental measurement of prototypes lead to the same conclusions as the numerical simulations made in Task 4.1.

1.3 The 3D Hilbert monopole: an example of 3D pre-fractal small antenna

The effective use of the radiansphere that encloses an antenna is supposed to reduce its quality factor approaching its value closer to the fundamental limit. Three-dimensional Hilbert pre-fractal monopole prototypes have been built as potential candidates to attain minimum Q factors for a given electrical size (Fig. III). However, the measurements reveal that, due to their large wires and their intricate topology, the increase in the ohmic resistance and the intense coupling reduce drastically the expected figures of the Q factor.

The experimental measurement of 3-D pre-fractal prototypes lead to the following conclusions:

- The space-filling property of Hilbert curves is highlighted in a three dimensional design, attaining higher miniaturization ratios (smaller electrical sizes) than with a planar configuration.

- The shape of the Hilbert pre-fractal provokes a strong cancellation of radiation, resulting in high Q values and small radiation resistances.

- The small radiation resistance along with the significant loss resistance of 3D Hilbert pre-fractal antennas makes them unpractical designs for a radiating system.

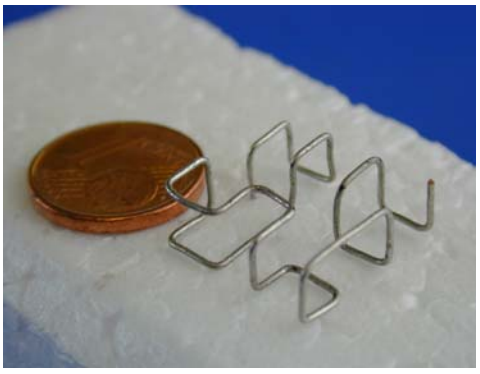

2nd iteration

h=5 mm
s=17 mm

3rd iteration

h=10 mm
s=23 mm

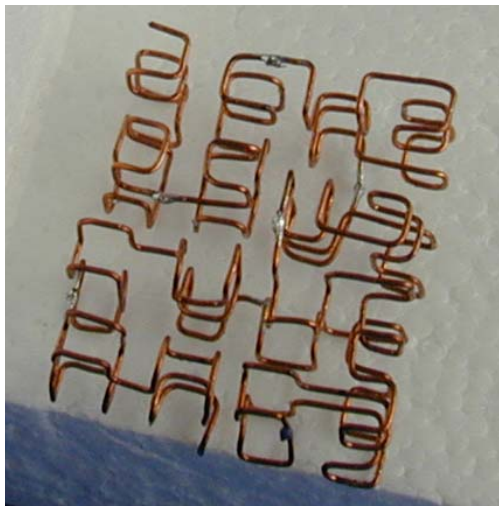

Figure III: Some of the 3D Hilbert monopole prototypes. The 10 eurocents coin is used as a reference for their size.

1.4 Prototypes and measurements at EPFL

Several prototypes of pre-fractal antennas and printed line fractal devices have been built and measured by the EPFL partner. The kind of measurements of these devices can be separated into three groups:

- The measurements of the reflection coefficient.
- The measurement of the radiation characteristics (radiation pattern, efficiency).
- Near field measurements for diagnosis purposes.

Measurement of small antennas radiation parameters

The EPFL partner has setup an unique facility for the measurement of small antenna parameters, in particular, loss efficiency and gain. Electrically small antennas are difficult to measure properly because they are neither purely symmetrical nor asymmetrical due to the limited size of ground planes or feeding baluns. Therefore, when the antenna is connected to a measuring device, a current flows in the outer conductor of the cable connecting the antenna, creating spurious radiation that completely masks the characteristics of the antenna under test. In order to overcome this problems, an original solution based on a random positioner has been developed (see Figure IV). Small antennas gain and loss efficiency can be accurately measured with the proposed solution.

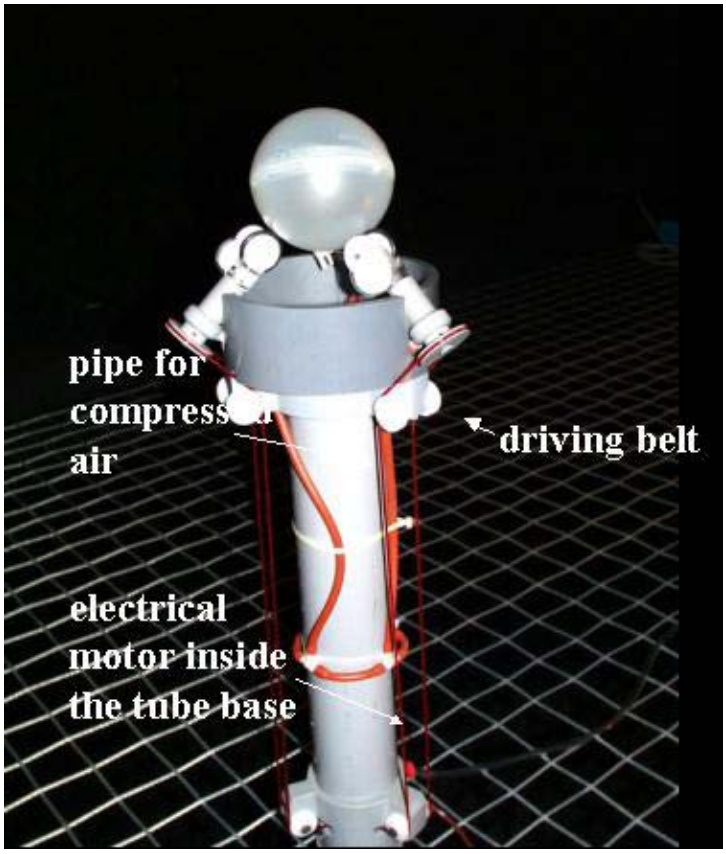

Figure IV: Random positioner for the measurement of small antennas at EPFL.

Near filed measurements

The EPFL has also used in this project a set up for measurement of the near field in the proximity of the antenna (Fig. V). This set-up uses a very small probe sensible to the three components of the electric field and is very useful for diagnostic purposes.

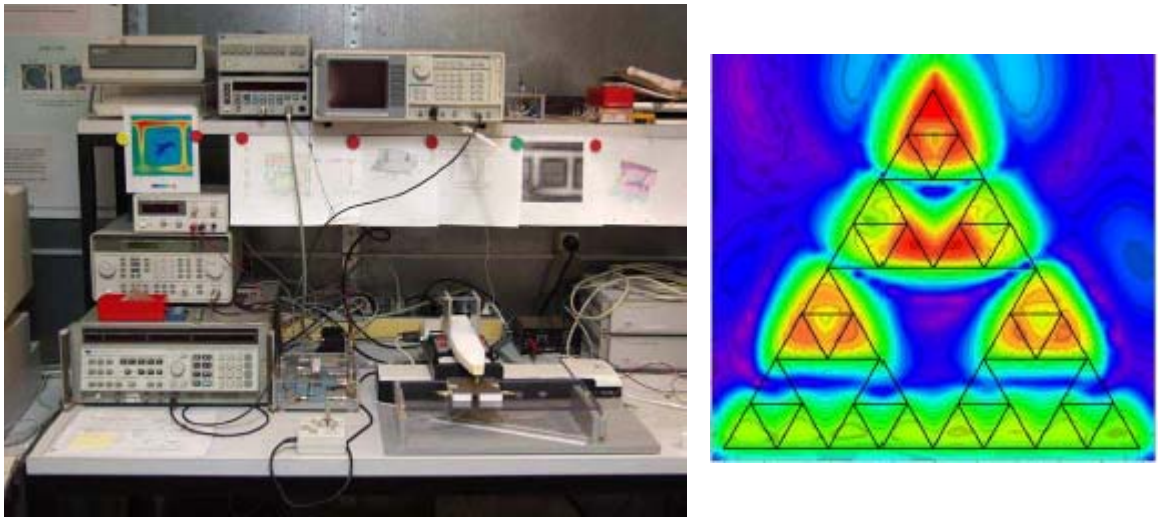

Figure V: Picture of the near-field measurement setup and near field measurements of the iteration 3 of a printed Sierpinski antenna.

Pre-fractal antenna prototypes

In this report three different families of microwave fractal-shaped devices are studied. The first two are based on well-known fractals, one is a surface fractal, the Sierpinski gasket, and one is a line fractal, the Koch curve, while the third is a new structure based on capillary filters.

The previously existing literature studies the Sierpinski as a monopole, as well as a patch. In the current contribution the measurements of a Sierpinski printed antenna are presented. The gaskets have been printed on a copper-berilium layer. To end the construction of these antennas the gaskets are going to be glued to a substrate of ε_r=1.07 and h=2mm and to a ground plane. The sticking process is going to be done with the help of a thin film of glue in order not to affect the permittivity of the substrate. The ground plane, the substrate, the film of glue and the gaskets are stacked and kept together with the help of two aluminum plates screwed tight.

a) 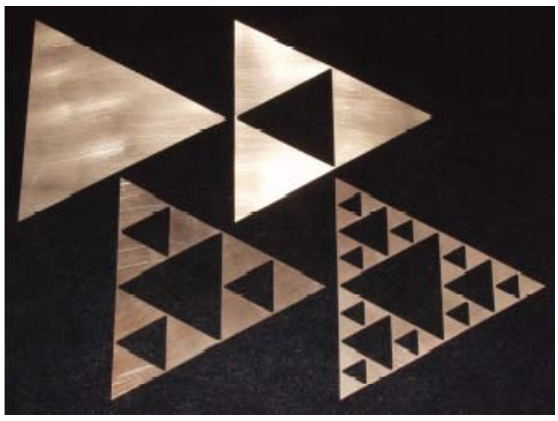 b) 

Figure VI: a) *Copper-berilium built Sierpinski gaskets, b) printed Sierpinski antennas.*

The Koch shaped devices studied in the existing literature are mainly based on the Koch monopole, but in the present report the study is done on different printed Koch-shaped structures (Fig. VII). The antennas have been printed on epoxy of thickness 0.1 mm and following the standard procedure for printed circuits. Once the Koch lines are printed on the epoxy, a brass ground plane, a substrate ε_r=1.07 of 3 mm of thickness and the epoxy with the printed lines are glued together in a hot glue process, as explained for the Sierpinski antennas.

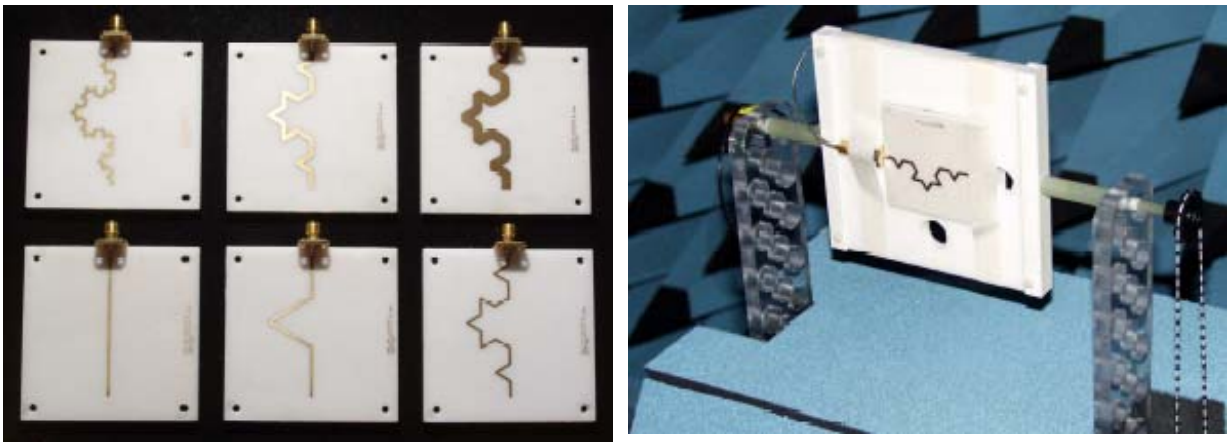

Figure VII: Printed Koch antenna prototypes and measurement set-up for the H-plane radiation pattern.

Finally, different line fractal shaped capillary filters belonging to the tree family have been built and measured (Fig. VIII).

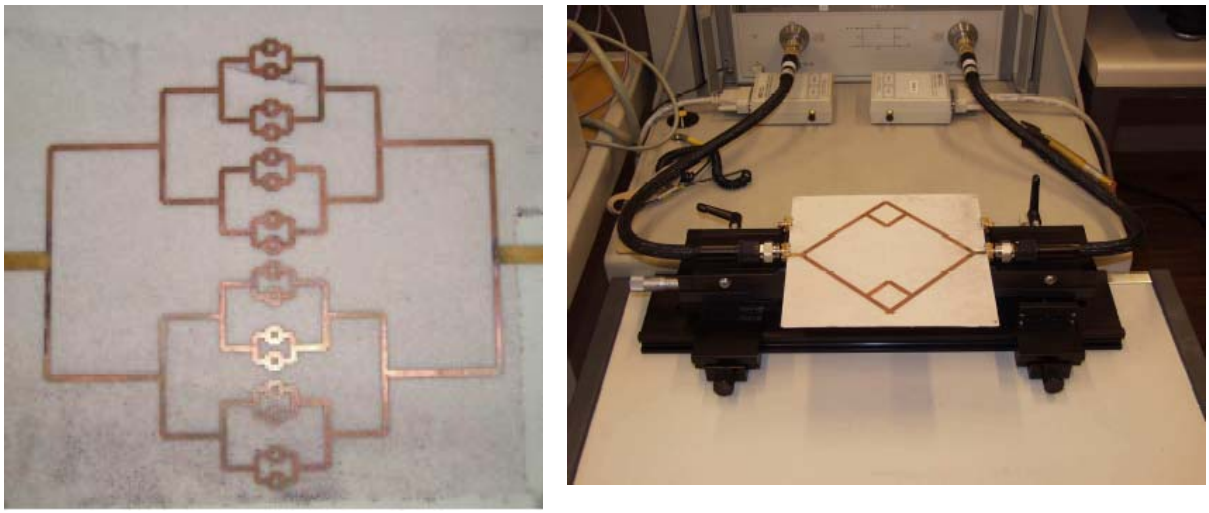

Figure VIII: 5th order square capillar filter and measurement set-up.

1.5 Task conclusions

Conclusions from this task are:

- The Wheeler cap method is an accurate, fast, and easy to implement technique for the measurement of radiation efficiency and quality factor of electrically small antennas.

- The Directivity/Gain method (in the near-field) can be also used to assess the measured results obtained with the Wheeler method because a measurement facility is accessible and measurement times are reasonable.

- A random positioner allows accurate measurement of antenna efficiency and maximum gain.

- Near field measurements show the field concentration at small parts of the antenna, typical from pre-fractal structures.

- Standard techniques for the fabrication of printed circuit boards are also useful for the manufacture of pre-fractal designs (technique used at UPC).

- Pre-fractal printed antennas can also be constructed by masking the shape on a copper-berilium layer and stacking the ground plane, the substrate, a thin film of glue and the gaskets (technique used at EPFL).

- For a given antenna size and length, non-fractal designs usually have lower measured resonance frequencies and wider bandwidths than pre-fractal monopoles, resulting in lower Q factor and higher efficiencies. Genetically designed pre-fractal antennas attain, in few cases, similar performances than conventional antennas.

- Three-dimensional pre-fractal design does not provide further improvements than planar design in the radiation performance of monopoles. In spite of the smaller electrical sizes attainable thanks to their increased space-filling capability, they have a more intricate topology and larger wires than their planar counterparts. Consequently, efficiency and Q factor for these 3D pre-fractals have unpractical values to real-world applications.

2 MEASUREMENT OF RADIATION EFFICIENCY AND QUALITY FACTOR OF FRACTAL ANTENNAS: THE WHEELER CAP METHOD

2.1 Introduction

The design of optimum electrically small antennas is still a challenging field. When designing electrically small antennas their radiation efficiency and their quality factor are the most outstanding parameters to take into account, because radiation pattern and directivity do not vary much for these small antennas.

In the following sections several methods for the measurement of radiation efficiency and quality factor of antennas are introduced. After a brief discussion the one that best fits our requirements will be selected and experimental results of its application to well-known antennas shown. Conclusions focused on the case of small fractal antennas are extracted in the last section of the document.

2.2 Glossary

AUT: Antenna Under Test
SEA: Standard Efficiency Antenna

2.3 Antenna efficiency measurement methods

The radiation efficiency η of an antenna is defined as the ratio of the radiated power P_{rad} to the input power P_{in}:

$$\eta = \frac{P_{rad}}{P_{in}} \tag{1}$$

This quantity can also be expressed as the quotient

$$\eta = \frac{P_{rad}}{P_{rad} + P_{loss}} = \frac{R_{rad}}{R_{rad} + R_{loss}} \tag{2}$$

where P_{loss} is the power dissipated on the antenna, R_{loss} is its loss resistance and R_{rad} is its radiation resistance. Both parameters in the denominator of expression (2) are easily measured as a whole (they are the real part of the input impedance of the antenna) but not easily separable, being difficult to measure the efficiency.

Various methods that could be used for measuring η have been described in the literature through the years. Among them are usually employed:

- the Wheeler cap method;
- the Directivity/Gain (also called pattern integration) method;
- and the Radiometric method.

2.3.1 The Wheeler Cap method

With this method the denominator of the expression (2) is determined from the measurement of the antenna input impedance Z_{in} using a network analyser.

Enclosing the antenna with a conducting sphere of radius equal to a radianlength ($\lambda/2\pi$) the radiation resistance R_{rad} will be eliminated from the input impedance [Wheeler, 1959] and without significantly changing the loss resistance R_{loss} (assuming that the conducting sphere does not change the current distribution on the antenna). Measuring in this case the input impedance Z_{wc} of the enclosed antenna R_{loss} is found:

$$\eta = \frac{\mathrm{Re}\{Z_{in}\} - \mathrm{Re}\{Z_{wc}\}}{\mathrm{Re}\{Z_{in}\}} \tag{3}$$

Consequently, using a network analyser and with two input impedance measurements (Z_{in} and Z_{wc}), one with a radiation shield and the other with the antenna in free space, the radiation efficiency is quickly and easily evaluated.

Expression (3) is useful when the input impedance of the antenna can be modelled by a series RLC (resistance-inductance-capacitance) circuit. When the model of the antenna is a parallel RLC circuit a variation in (3) has to be used

$$\eta = \frac{\mathrm{Re}\{Z_{in}\}}{\mathrm{Re}\{Z_{in}\} - \mathrm{Re}\{Z_{wc}\}} \tag{4}$$

When the loss mechanism is even more complicated the Wheeler cap method is not a valid technique to determine efficiency ([Pozar, 1988]). To overcome this limitation, a rotation of the reflection coefficients is proposed by McKinzie at [McKinzie III, 1997] (the same angle for the free space and Wheeler cap reflection coefficients). The rotation is equivalent to adding a fictitious lossless transmission line to the antenna input. Proceeding this way the resonant frequency of the antenna will also be its matching frequency and the new input impedance representation on the Smith chart will be tangent to a constant resistance contour. At resonance this means a good approximation of a series RLC circuit. If the rotation angle needed to match the resonant frequency and the matching frequency is π, the well-approximated circuit at resonance is a parallel RLC. Experimental results where this method was used agree within 1% with more complex post processing methods ([McKinzie III, 1997]).

Experiences ([Newman, 1975], [Pozar, 1988], [Chair, 2002]) using this method are reflected in the following considerations to take into account when making measurements:

- the shape of the conducting cap is not critical (theoretical approach at [Huang, 2001]);
- the cap has to make good electrical contact with the ground plane when working with monopole antennas;
- it is not necessary to have the cap perfectly centred over the antenna;

- the room in which the measurement takes place could cause significant changes in input impedance.

The Wheeler cap method is limited by the size of the cap when working in the low frequency range and by the uncertainties (after calibration) of the network analyser when small radiation resistances are measured ([Ida, 1999]).

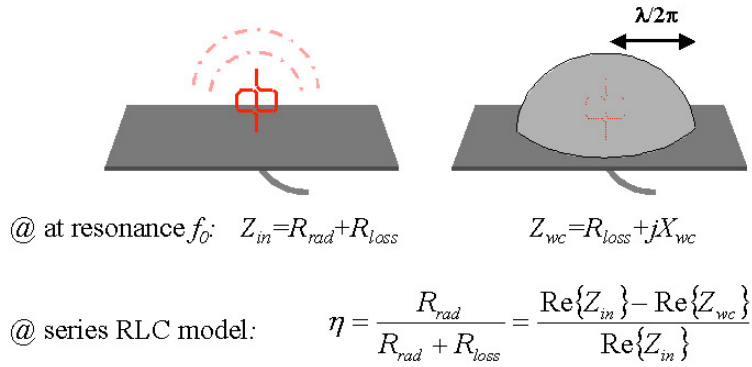

Figure 1. Scheme of the Wheeler Cap Method.

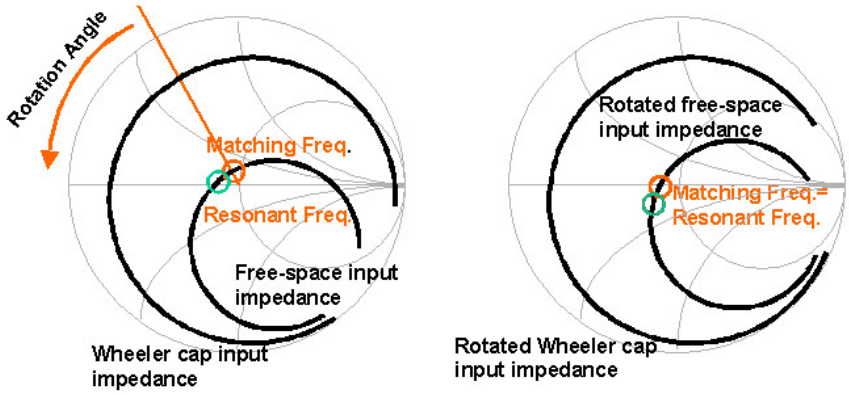

Figure 2. (a) Typical measured reflection coefficient "not well modelled" by a RLC circuit and (b) rotated measurements.

When using the Wheeler method we have to assure that at the operating frequency f_0 the conductivity σ_s of the shield is high enough for the skin depth d_s to be greater than the thickness t of the shield.

$$t >> d_s = \sqrt{\frac{1}{\pi f_0 \mu_s \sigma_s}} \tag{5}$$

2.3.2 The Directivity/Gain method

It is an indirect method to measure the radiation efficiency from the quotient:

$$\eta = \frac{G}{D} \tag{6}$$

where G is the gain of the AUT (measured using a standard gain horn), and D is the directivity of the AUT.

Directivity could be determined from the expression

$$D = \frac{41253}{\Delta\theta\,\Delta\phi} \tag{7}$$

being $\Delta\theta$ and $\Delta\phi$ the principal plane beamwidths (in decimal degrees) measured from the radiation pattern of the antenna. This expression is pretty useful when high gain antennas are under test.

A more accurate technique used to extend the method to any kind of antennas and to cancel common errors in the measurement process is the integration of the measured pattern data. In this sense, the Directivity/Gain method is also known as the pattern integration method. It is based on the measurement of the input power P_{in} to the AUT and the radiated power P_{rad} by the antenna. The power radiated is measured from the integration of the normal component of the time average Poynting vector over a closed surface that surrounds the antenna. Being the surface a sphere of radius r, in the far zone, the efficiency is evaluated as ([Smith, 1977])

$$\eta = \frac{\dfrac{r^2}{2Z_0}\oint\left(\left|E_\phi^r\right|^2 + \left|E_\theta^r\right|^2\right)d\Omega}{P_{in}} \tag{8}$$

where $E^r{}_\phi$ and $E^r{}_\theta$ are the electric field components tangential to the surface of the surrounding sphere, and Z_0 is the characteristic impedance of free space.

Sources of error of the method are:

- the accurate measurement of the gain is difficult;
- the losses and/or mismatch of the transmitter waveguide to coaxial when using a standard gain horn;
- lack of repeatability due to positioning of the AUT in the measurement set-up;
- slowness of the method when using pattern integration and not small antennas;
- the radiation/interference problems with the antenna mount and feed cable, when measuring small antennas ([Johnston, 1998]) in the far field.

2.3.3 Radiometric measurement of radiation efficiency

This technique is based on the fact that a lossy antenna pointing at a cold target will generate less noise power than a less lossy antenna pointed at the same target (the losses of the antenna behave as a noise source at ambient temperature).

Radiation efficiency is measured as the quotient ([Pozar, 1988]) of:

$$\eta = \frac{\delta(\varepsilon - 1)}{\varepsilon(\delta - 1)} \tag{9}$$

where ε is

$$\varepsilon = \frac{P_w}{P_c} \tag{10}$$

being P_w the ratio among the noise power of the antenna under test when placed in an anechoic chamber (at a temperature of about 290ºK) and P_c is the noise power measured by the antenna when directed toward the clear sky (it behaves as a cold target at about 5ºK).

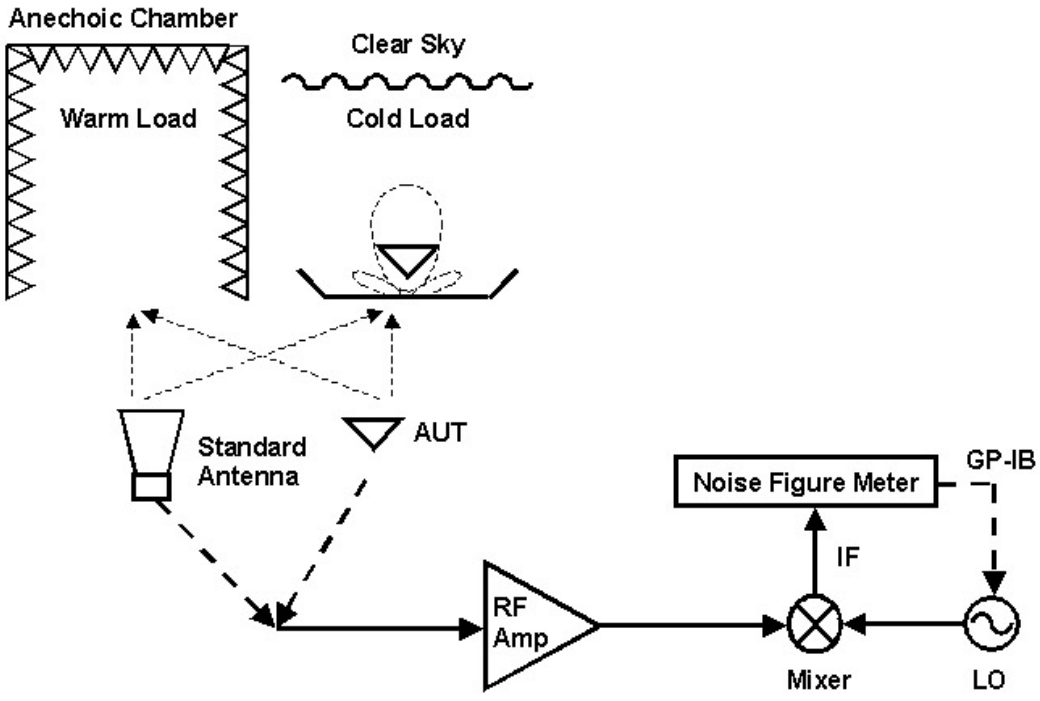

Figure 3. Scheme of the Radiometric method of efficiency measurement.

The parameter δ is a quotient used to correct the effect of the system noise (the noise generated by the circuitry). The measurement of the quotient P_w/P_c is repeated, but using a waveguide horn as a "standard" antenna which can be assumed to have η=1.

A more detailed description of the mathematics involved in the method can be found at [Ashkenazy, 1988].

The main problems associated with this technique is the lowering of the apparent efficiency of the AUT due to:

- the fact that all of the antenna pattern should point to the noise source when measuring the clear sky, so a metallic reflector has to be used to help the off-broadside pattern to "see" the sky;
- the external circuitry should have good noise figures and be mounted close to the AUT;
- the mismatch among antenna and circuitry;
- the drift of the amplifier gain translates to errors on η.

This method is the more complex and requires accurate components and care when measuring.

2.3.4 Another methods

Another techniques less referenced in the literature follow. New ones are still under consideration ([Johnston, 1996] and [Johnston, 1998]).

2.3.4.1 The Q method

An easy and quick method to use for the measurement of the radiation efficiency is the *Q* method ([Newman, 1975]). Efficiency is evaluated as the ratio of the quality factor of a realizable antenna Q_{RL} (including radiated and dissipated power) and the quality factor of an ideal antenna Q_R identical to the realizable but with conductors with perfect conductivity and dielectrics without losses,

$$\eta = \frac{Q_{RL}}{Q_R} \tag{11}$$

While Q_{RL} can be measured with a network analyser, Q_R is determined from the expression of the fundamental limit as a function of *ka*, where *k* is the wavelength number at resonance and *a* is the radius of the smallest sphere that encloses the antenna (and its image in the case of monopoles). The fundamental limit for a linearly polarized small antenna was devised by L.J. Chu ([Chu, 1948], [Hansen, 1981]) and later re-examined by J.S. McLean ([McLean, 1996]),

$$Q_R = \frac{1}{ka} + \frac{1}{(ka)^3} \tag{12}$$

An exact determination of the quality factor of the ideal antenna Q_R should consider all the supporting structures of the antenna and the precise distribution of spherical waveguide modes radiated by this complex structure.

This approximation fails for not small antennas. Taking as reference the experiences of E.H. Newman ([Newman, 1975]) the approximation fails for $ka>0.2$.

2.3.4.2 The Random Field Measurement technique

J.B. Andersen ([Andersen, 1977]) proposed an outdoor technique for the measurement of the radiation efficiency (not very extended in the literature) called Random Field Measurement (RFM) technique. It is based on the assumption that the cumulative probability of reception should be the same, such as a Rayleigh distribution, for the AUT and for a reference antenna with known radiation efficiency and.

In the ’80, some modifications to the original method were introduced in order to use the technique in an indoor environment and overcoming some of the cons (large measurement times and large transmitting powers) of the original method. In this sense the indoor technique could be used in an office room or a laboratory (previously *designed* to assure a Rayleigh distribution with independently of polarization, [Maeda, 1988]).

The cumulative probability of reception versus relative receiving power from a Standard Efficiency Antenna (SEA) is measured using a rotating receiving antenna. Both antennas are in the same room with the transmitting antenna (the SEA) surrounded by radio wave scatterers.

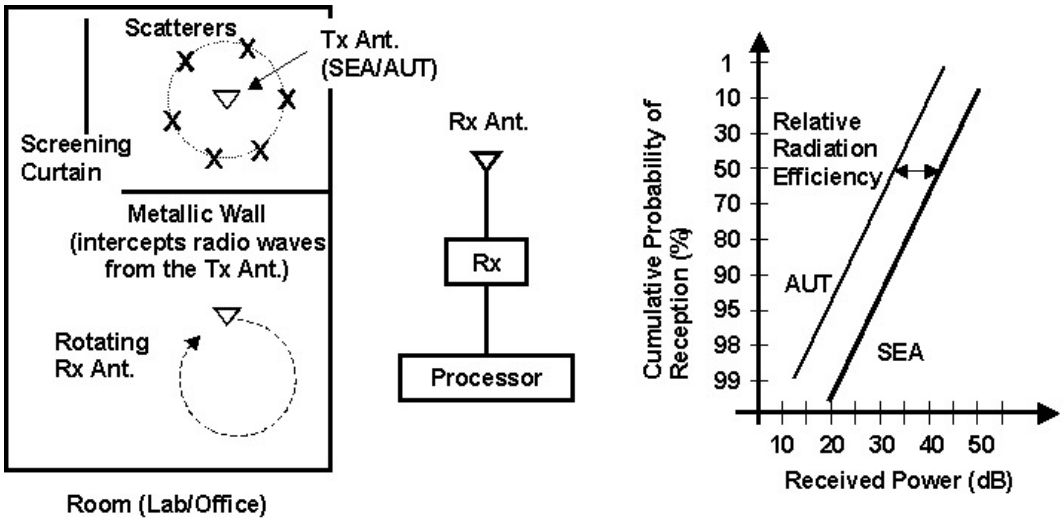

Figure 4. Scheme of the Random Field Measurement technique.

The measurement process is repeated but now using the AUT. In this measurements the cumulative probabilities of reception of SEA and AUT should have the same distribution. The relative radiation efficiency of the AUT is determined from the difference between the received power of the AUT and that of the SEA, corresponding to the same cumulative probability of reception, such as 50% ([Maeda, 1988]).

The radiation efficiency measured using this technique includes the reflection losses of the antenna.

The radiation efficiency of an antenna does not depend on the set up direction of the antenna, so the mean value of the receiving power for the antenna should be constant even if the set up direction is changed.

2.3.4.3 Resistance comparison method

Two identical antennas are constructed except that they are fabricated with different metals (σ_1, μ_1 and σ_2, μ_2). Both antennas will have different efficiencies η_1 and η_2

$$\eta_1 = \frac{R_{rad1}}{R_{rad1} + R_{loss1}} \qquad \eta_2 = \frac{R_{rad2}}{R_{rad2} + R_{loss2}} \qquad \text{(13) and (14)}$$

but radiation resistance is the same for both (R_{rad1}=R_{rad2}). Ohmic resistances differ by a multiplicative constant γ. If frequency is high enough the concept of surface resistance R_S can be used, and the constant is:

$$\gamma = \frac{R_{loss2}}{R_{loss1}} = \frac{R_{S2}}{R_{S1}} = \sqrt{\frac{\sigma_1 \mu_2}{\sigma_2 \mu_1}} \qquad (15)$$

The radiation efficiency is determined from the measured values of the input resistance (R_{in1}=R_{rad1}+R_{loss1} and R_{in2}=R_{rad2}+R_{loss2}) of both antennas

$$\eta_1 = \left(\frac{R_{in2}}{R_{in1}} - \gamma \right) \Big/ (1 - \gamma) \qquad (16)$$

2.4 Quality factor measurement methods

The quality factor Q of an electrical network at resonance may be defined as

$$Q = \frac{\omega W}{P} \qquad (17)$$

where P is the power dissipated in the network, W is the time-average energy stored in it, and ω is 2π times the working frequency (the radian frequency).

When the network is not resonant an additional ideal lossless reactive element is needed so that the input impedance is purely real at a specific design frequency. For an antenna, it is commonly accepted the following definition of Q ([Collin, 1964], [McLean, 1996])

$$Q = \frac{2\omega W_e}{P_{rad}} \qquad W_e > W_m \tag{18}$$

$$Q = \frac{2\omega W_m}{P_{rad}} \qquad W_m > W_e \tag{19}$$

being W_e the time-average, non-propagating, stored electric energy, W_m the time-average, nonpropagating, stored magnetic energy and P_{rad} the radiated power.

The quality factor is a parameter that specifies the performance of the antenna. A high value of Q means that there are large amounts of reactive energy stored in the near zone field. Large currents, high ohmic losses, narrow bandwidths and large frequency sensitivity are also consequences of a high Q value.

The evaluation of the average stored electric and magnetic energy could be done establishing the relation between antennas and one-terminal microwave networks. In this case the Q factor can be computed as

$$Q = \frac{\omega}{2R_{rad}}\left(\frac{dX_{in}}{d\omega} + \left|\frac{X_{in}}{\omega}\right|\right) \tag{20}$$

being X_{in} the reactance of the antenna in free-space and R_{rad} the radiation resistance of the antenna.

If the Q is high it can be interpreted as the inverse of the fractional bandwidth of the input impedance of the antenna, defined as the normalized spread between the half-power frequencies

$$Q = \frac{f_0}{\Delta f} = \frac{f_{center}}{f_{upper} - f_{lower}} \tag{21}$$

For Q<2 the previous representation is no longer accurate [Hansen, 1981].

For an ideal lossless antenna its Q could be evaluated from the quotient among its resonant frequency and the bandwidth between the frequencies for which the resistance is equal to the reactance [Newman, 1975]. If the antenna is matched to a transmission line the half power frequencies that determine Δf occur for a power reflection coefficient of 0.5 (SWR=5.83).

For a real antenna the Q factor could be measured using a network analyser. For instance, in [Altshuler, 2002] the Q factor was measured using the expression in (21) but being f_{center} the frequency at resonance and f_{upper} and f_{lower} the frequencies around f_{center} where conductance dropped to ½ from the conductance at resonance.

Both methods measure the Q factor of a lossy antenna, so when comparing the results with the fundamental limit we have to be careful with the interpretation of the results because antennas could give values under the fundamental limit.

If we were able to measure the ohmic resistance R_{loss} separately from the input impedance of the antenna $R_{in}+jX_{in}$ ($R_{in}=R_{rad}+R_{loss}$), the ideal antenna (lossless) Q factor could be evaluated from the expression

$$Q = \frac{\omega}{2\left(R_{in} - R_{loss}\right)}\left(\frac{dX_{in}}{d\omega} + \left|\frac{X_{in}}{\omega}\right|\right) \tag{22}$$

where R_{in}-R_{loss} is the radiation resistance and X_{in} the reactance of the AUT.

Other recent method for the measurement of Q for microstrip antennas is based on scattering measurements and it is shown at [Weiss, 2000].

2.5 Selection of the methods for the determination of radiation efficiency and quality factor

Accordingly to the methods reviewed in the previous sections, the technique that will be used in the Fractalcoms project is the Wheeler cap method.

2.5.1 Why the Wheeler cap method?

From the experiences related in the literature, the technique that best fits in our investigation is the Wheeler cap method. Several characteristics make it very appealing and suitable to our needs:

- although may be deficient from a theoretical point of view ([Pozar, 1988]) in practice, several authors confirm the good agreement with expectations ([Newman, 1975], even [Pozar, 1988]);
- it gives repeatable results: ±2% according to [Pozar, 1988]. Another authors confirms these results using the same methods and caps with different sizes ([Chair, 2002]) and materials (also differences of ±2% in [Newman, 1975]) ;
- it is the easiest to implement;
- accuracy of the method is improved using the post processing proposed by McKinzie III [McKinzie, 1997];
- not only efficiency can be measured using the method, but also the ideal lossless quality factor Q thanks to the direct determination of the ohmic losses R_{loss} of the antenna under test. The lossless Q can be compared with the fundamental limit of antennas stated by Chu ([Chu, 1948]) and reviewed by McLean ([McLean, 1996]).

Though the Directivity/Gain is the potentially better method it seems that it is the least accurate and repeatable according to [Pozar, 1988] results. The radiometric method is in between with the Wheeler method. Its potentiality is based in the fact that it does not rely on any assumption that limits its accuracy and range of application.

The Wheeler cap method is very useful for making a quick experimental characterization and optimisation of antennas (in the sense of its radiation efficiency) because of its simplicity and easy of measurement.

In the case of small antennas the large measurement times of the Directivity/Gain method are dramatically reduced due to the small quantity of spherical modes that really mean in the far field, so using a near field spherical scanning system the number of samples needed to retrieve a whole radiation pattern is very small. This near field technique has to be considered as an alternative to verify doubtful results with other methods.

2.5.2 Measurement procedure and measurement set-up

The measurement procedures for radiation efficiency and quality factor determination are explained in the following sections.

2.5.2.1 Measurement procedure

The antenna under test is connected to the pin of a 2.4 mm SMA connector attached to a ground plane of 80x80 cm^2 and 3 mm width. Using an HP 8753D network analyser the input impedance of the AUT in free space Z_{in} is measured

$$Z_{in} = R_{in} + jX_{in} = R_{rad} + R_{loss} + jX_{in} \tag{23}$$

A cap is fabricated or acquired according to the measurement range of the AUT (some examples of caps are shown is section 6.2.2).

Attaching the cap to the ground plane with fixing screws (proceeding this way a good electrical contact between the cap and the ground plane is assumed) the input impedance of the enclosed AUT Z_{wc} is measured using the network analyser.

$$Z_{wc} = R_{wc} + jX_{wc} = R_{loss} + jX_{wc} \tag{24}$$

Radiation efficiency and quality factor are calculated from both measurements and the following equations

$$\eta = \frac{\mathrm{Re}\{Z_{in}\} - \mathrm{Re}\{Z_{wc}\}}{\mathrm{Re}\{Z_{in}\}} = \frac{R_{rad}}{R_{rad} + R_{loss}} \qquad \text{(3) and (2)}$$

$$Q = \frac{\omega}{2\left(\mathrm{Re}\{Z_{in}\} - \mathrm{Re}\{Z_{wc}\}\right)}\left(\frac{d\,\mathrm{Im}\{Z_{in}\}}{d\omega} + \left|\frac{\mathrm{Im}\{Z_{in}\}}{\omega}\right|\right) = \frac{\omega}{2R_{rad}}\left(\frac{dX_{in}}{d\omega} + \left|\frac{X_{in}}{\omega}\right|\right) \qquad \text{(25) and (26)}$$

The input impedance of the antenna should be measured in an anechoic chamber, because its value depends on the power reflected back to the antenna from the environment.

2.5.2.2 *Examples of caps (radiant shields)*

When using a radiating shield to measure the radiation efficiency and quality factor with the Wheeler method, the lowest working frequency is determined by the size of the cap and the radianlength (in a spherical cap $a=\lambda/2\pi$, being a the radius of the cap). As Wheeler stated, neither size, shape nor electrical conductivity of the cap are critical, because it is assumed that the current distribution on the antenna is not changed when the radiating shield surrounds it. [Smith, 1977] demonstrated that the size of the cap can even be smaller than the radianlength $\lambda/2\pi$ if the loss tangent of the cap material, $\sigma/\omega\varepsilon$, is high enough. In the high frequency range the measured η and Q could be affected by the presence of resonant modes.

In order to investigate the frequency operating ranges and the influence of shape and size of the Wheeler cap in the results, different aluminium (conductivity $\sigma_s=3.8\cdot10^{-7}$ $\Omega^{-1}m^{-1}$) caps have been acquired and tested using a $\lambda/4$ monopole as AUT. Figure 5 shows the four caps analysed: two spherical caps with radii 100 mm and 130 mm, a rectangular cap of dimensions 66x66x180 mm^3, and a 125 mm high cylindrical cap of 30 mm radius. Thickness of the walls of the caps are 1 mm for the spherical caps, 2 mm for the rectangular, and 5 mm for the cylindrical.

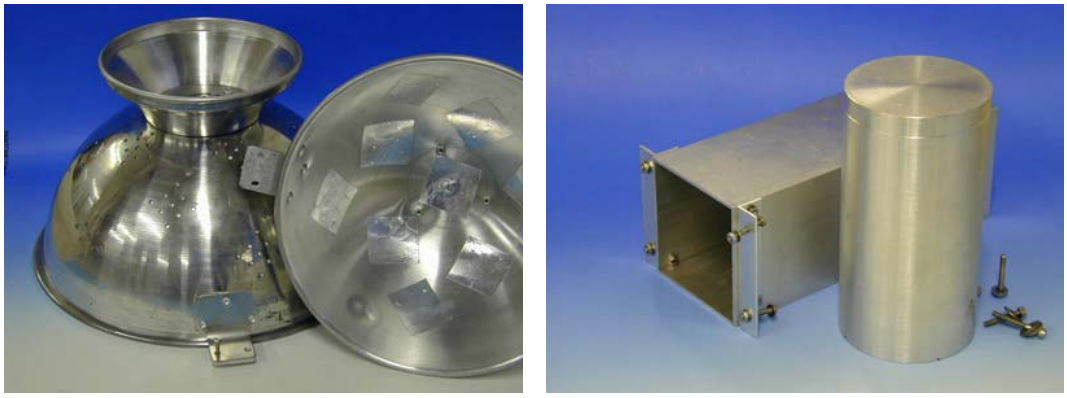

Figure 5. (a) Spherical caps with radii 100 mm and 130 mm; (b) cylindrical cap with radius 30 mm and 120 mm high, and rectangular cavity of 66x66x180 mm^3.

Figure 6 shows the return losses when the rectangular cap is excited with a monopole of 100 mm (first resonance at 750 MHz), centrally mounted and skewed 10º towards a corner of the cap ([Austin, 1989]). Various resonant modes of the cavity are clearly visible. Their theoretical values are obtained from the classical expression (adapted from [Henney, 1959])

$$f_{mnp} = \frac{c}{2\pi}\sqrt{\left(\frac{m\pi}{a}\right)^2 + \left(\frac{n\pi}{b}\right)^2 + \left(\frac{p\pi}{h}\right)^2} \tag{27}$$

where *a* and *b* are the dimensions of the base of the cavity, and *h* is its height. *m*,*n* and *p* are the number of half-wave variations of the field along their respective axis. These numbers are integers including 0, but not more than one may equal 0 for fields to exist. Modes 0*np* and *m*0*p* with *m*=*n* are equal.

Resonant mode at 2.42 GHz (011) limits the frequency range at which this cap can be used. To avoid serious errors in the measured radiation efficiency a guard-band around it has to be provided.

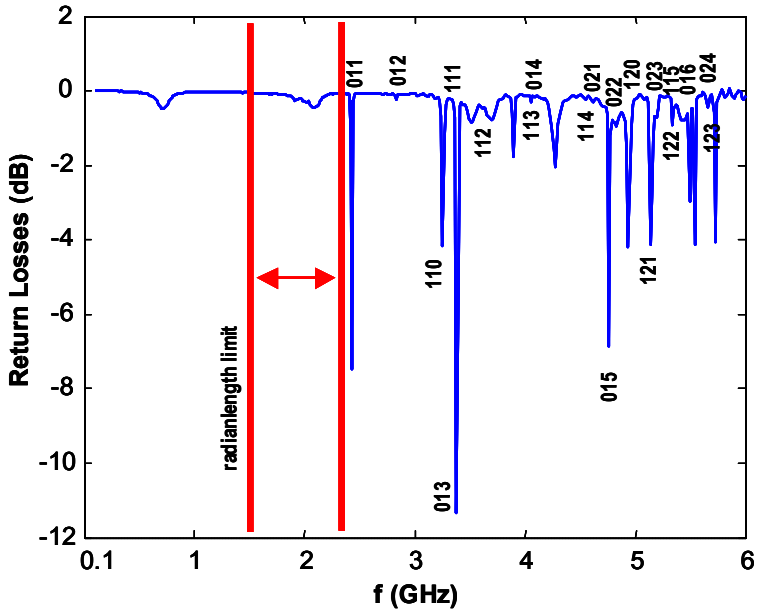

Figure 6. Return losses of the rectangular cavity. Modes associated with the resonances are shown. The useful frequency range of the cavity is also presented.

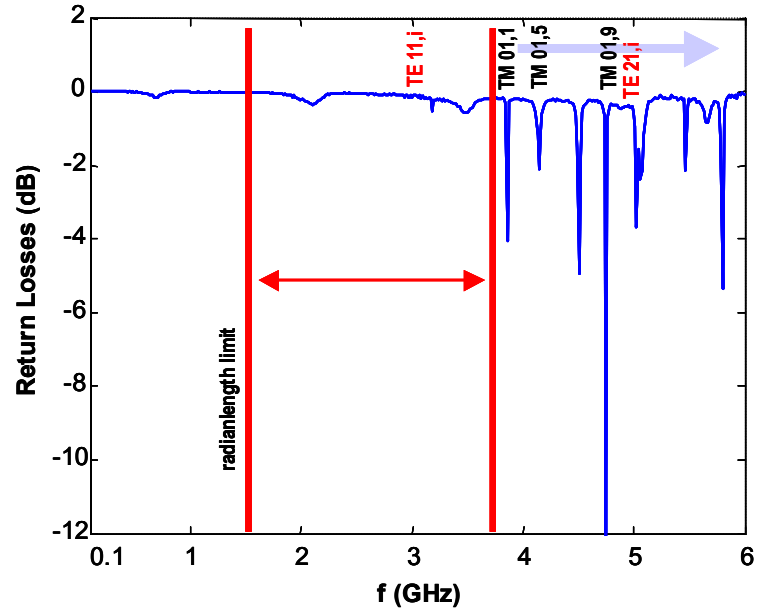

Figure 7. Return losses of the cylindrical cavity. Modes associated with the resonances are shown. The useful frequency range of the cavity is also presented.

Figure 7 shows the return losses when the cylindrical cap with height 120 mm and radius 30 mm is used, and the skewed monopole resonant at 750 MHz (100 mm height) is the excitation. Useful range of measurement is just below a $TM_{01,1}$ mode at nearly 3.84 GHz.

For a cylindrical resonator the infinite number of resonant modes could be divided into *TE* modes (field transverse to the axis of the cylinder) and *TM* modes (magnetic field transverse to the axis of the cylinder and electric field with an axial component). *TE* modes are at frequencies

$$f_{mn,p} = \frac{c}{4}\sqrt{\frac{2p}{h} + \left(\frac{2u'_{m,n}}{\pi a}\right)^2} \tag{28}$$

where h and a are respectively the height and radius of the cylinder, p is the integral number of λ/2 along the axis of the cylinder (p=0 excluded), and $u'_{m,n}$ is the nth root of the equation

$$J'_m(u') = 0 \tag{29}$$

being $J'_m(x)$ the first derivative of the Bessel function of order m.

TM mode resonant frequencies are at

$$f_{mn,p} = \frac{c}{4}\sqrt{\left(\frac{2p}{h}\right)^2 + \left(\frac{2u_{m,n}}{\pi a}\right)^2} \tag{30}$$

where now p admits 0, and $u_{m,n}$ is the nth root of the equation

$$J_m(u) = 0 \tag{31}$$

being $J_m(x)$ the Bessel function of order m.

Figures 6 and 7 also show the resonances of the exciting monopole (at ~0.75 GHz, ~2.1 GHz and ~3.5 GHz for the rectangular and cylindrical cavities). Frequencies are slightly deviated due to the effect of the cap on the input impedance of the monopole.

For a spherical cavity the mode that limits the use of the Wheeler method is the TM_{101}. This mode is found at

$$f = \frac{c}{2.29a} \tag{32}$$

where a is the cavity radius. The next longest mode is the TE_{101} at

$$f = \frac{c}{1.395a} \tag{33}$$

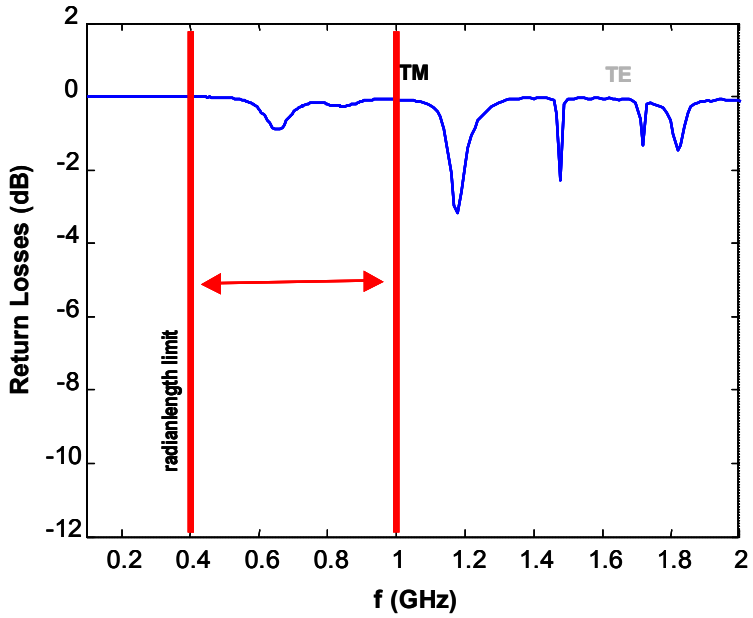

Figure 8. Return losses of the hemispherical cavity with a=130 mm.

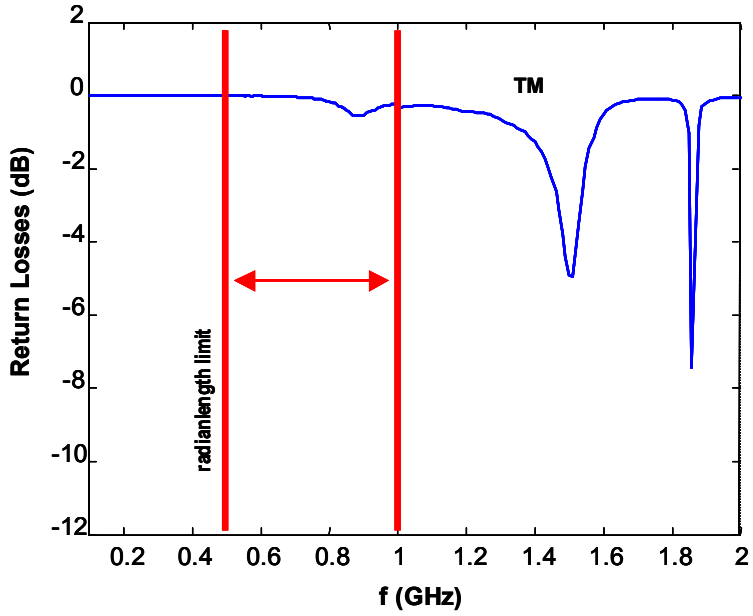

Figure 9. Return losses of the hemispherical cavity with a=100 mm.

Figure 8 shows the return losses for a hemispherical resonator with radius a=130 mm. The first resonance is shifted to a higher band (than expected) at ~1.1 GHz probably due to the effect of the ground plane truncation of the sphere. When a small hemisphere, a=100 mm, is used the first resonance is also at a high frequency than expected, ~1.5 GHz, but a wider guard-band has to be provided. In this case the excitation was also a

skewed monopole but now resonant nearly 1 GHz. Return losses of this structure is at figure 9.

Figures 8 and 9 also show the resonances of the exciting monopole.

According to the measured resonances of the cavities (figures 6, 7, 8, 9) that limit their upper usable frequencies working as caps, and the limiting lower frequencies defined by the radianlegth ($\lambda/2\pi$) criterion, the operating ranges for the measured caps are approximately (including guard-bands):

- rectangular cap: 1.5 - 2.4 GHz;
- cylindrical cap: 1.6 - 3.5 GHz;
- spherical cap with a=100 mm: 0.5 – 1.0 GHz;
- spherical cap with a=130 mm: 0.4 – 1.0 GHz.

2.5.2.3 Testing the method with a monopole

Some tests about accuracy of the Wheeler method were carried out when the caps shown in the previous section were used. Also the effect of shifting the cap from the centre of the antenna was studied empirically (note that most of the pre-fractal structures that we are going to characterize have not axes of symmetry). Measurements of repeatability are well documented in the literature and considered unnecessary into this report.

Two $\lambda/4$ monopoles are measured in terms of efficiency and quality factor using the rectangular and cylindrical caps and with the standard processing method stated by Wheeler and the proposed by McKinzie III. The monopoles are 35 mm and 28 mm height, to be resonant at 2.0 GHz and 2.5 GHz. Both are fabricated with a cupper wire of 0.25 mm radius wire. Previously the monopoles were simulated using a method of moments code, NEC2D, and their results compared with the measurements. Efficiencies and quality factors of both monopoles are presented in tables 1 and 2 and compared with simulated results.

Monopole 35 mm 2.0 GHz	Simulated η	η (Wheeler)	η (McKinzie)	Simulated Q	Q (Wheeler)	Q (McKinzie)
Rectangular Cap	99.6 %	96.4 %	98.6 %	5.5	5.8	3.1
Cylindrical Cap	99.6 %	90.4 %	94.9 %	5.5	6.2	3.3

Table 1. Theoretical and measured η and Q for the monopole of 35 mm.

Monopole 28 mm 2.5 GHz	Simulated η	η (Wheeler)	η (McKinzie)	Simulated Q	Q (Wheeler)	Q (McKinzie)
Rectangular Cap	99.6 %	84.2 %	98.5 %	5.2	3.2	5.8
Cylindrical Cap	99.6 %	96.7 %	99.6 %	5.2	2.8	5.7

Table 2. Theoretical and measured η and Q for the monopole of 28 mm.

As expected, when the working frequency of the monopole is in the centre of the operating range of the caps, the results are more accurate in terms of radiation efficiency. In this sense, the cap suitable for the measurement of the monopole of 35 mm is the rectangular, and the cap suitable for the measurement of the monopole of 30 mm is the cylindrical. Results are more accurate when using the post processing technique of McKinzie III.

Differences among models and real antennas make accuracy of quality factor more difficult to achieve. In any case results are quite consistent to use the method.

Other set of measurements in relation with the influence of the relative position between the centre of the antenna under test and the centre of the cap were carried out. Tables 3 and 4 show the input resistance, ohmic losses, efficiency and quality factor of a $\lambda/4$ monopole when measured with the Wheeler cap method using the *standard* post processing and the specified by McKinzie III. The whole measurements were carried out with the cap not screwed to the ground plane but assuring a good electrical contact with it. Nevertheless, the slight differences between the measured results and with their respective values in tables 1 and 2 (when the cap and the AUT are both centred and screwed) show the great importance of the good electrical contact between cap and ground plane.

$\lambda/4$ monopole ~2.5 GHz Cylindrical cap	Wheeler method				McKinzie post processing			
ΔR (mm) off the centre	$R_{rad}+R_\Omega$ (Ω)	R_Ω (Ω)	η (%)	Q	R_r+R_Ω (Ω)	R_Ω (Ω)	η (%)	Q
0	19.9	1.0	94.9	4.9	36.4	0.7	98.0	2.9
5	19.9	0.9	95.3	4.9	36.4	0.5	98.7	2.9
10	19.9	0.8	95.9	4.9	36.4	0.5	98.7	2.9
15	19.9	0.8	96.2	4.8	36.4	0.6	98.5	2.9
20	19.9	0.8	96.0	4.9	36.4	0.7	98.1	2.9
22	19.9	0.9	95.5	4.9	36.4	0.9	97.5	2.9
23	19.9	1.2	93.8	5.0	36.4	1.0	97.2	3.0

Table 3. Measured η and Q of a $\lambda/4$ monopole matched at 2.5 GHz and using the cylindrical cap.

Once, measurements post processed with the method of McKinzie are more precise than the standard Wheeler method. Input resistances and efficiencies get with this technique are closer to the expectations for a $\lambda/4$ self-resonant monopole.

As tables 3 and 4 show the shifting between antenna centre and cap centre does not have influence on the results (while the cavity walls are not very close to the antenna).

$\lambda/4$ monopole ~2.0 GHz Rectangular cap	Wheeler method				McKinzie post processing			
Δx (mm) - Δy (mm) off the centre	$R_{rad}+R_\Omega$ (Ω)	R_Ω (Ω)	η (%)	Q	R_r+R_Ω (Ω)	R_Ω (Ω)	η (%)	Q
0 – 0	25.4	0.8	96.8	5.0	37.6	0.4	98.9	3.2
5 – 0	25.4	0.8	96.8	5.0	37.6	0.4	98.9	3.2
10 – 0	25.4	1.0	96.1	5.0	37.6	0.5	98.6	3.2
15 – 0	25.4	0.8	96.9	5.0	37.6	0.7	98.1	3.3
20 – 0	25.4	1.0	96.0	5.0	37.6	1.0	97.3	3.3
5 – 5	25.4	0.7	97.2	5.0	37.6	0.5	98.7	3.2
10 – 10	25.4	4.3	83.2	5.8	37.6	0.9	97.5	3.3
15 – 15	25.4	1.4	94.6	5.1	37.6	0.6	98.3	3.3
20 – 20	25.4	0.7	97.4	5.0	37.6	0.7	98.1	3.3

Table 4. Measured η and Q of a $\lambda/4$ monopole matched at 2.0 GHz and using the rectangular cap.

Measurements on the behaviour of a spherical cap when excited with a $\lambda/4$ monopole deserve especial attention. Conditions that define the working range as a cap specify a narrow frequency band not very useful in practice in the case of *tall* structures. The lower limit of operation as a cap is determined, as other cavities, by the radianlength and the radius of the cap ($a \geq \lambda/2\pi$), and the higher frequency of operation is limited by the first resonant frequency at the TM_{101} mode ($\lambda > 2.29a$). The first condition is always accomplished if the cavity has to accommodate a $\lambda/4$ monopole. Equation (34) briefs both conditions

$$0.25\lambda \leq a < 0.43\lambda \tag{34}$$

Consequently, the provision of a guard-band around the upper frequency limit reduces the operating frequency range of the spherical cap (and also the hemispherical cap) and even not very accurate results are expected when working with tall structures due to the closeness of the metallic cap to the higher parts of the AUT. This expectations were assessed verified when measuring a $\lambda/4$ monopole fabricated with a 94 mm high and 0.5 mm diameter cupper wire matched at 0.76 GHz. While its simulated (with NEC2D) efficiency was 99.4%, the measured efficiency with the small cap of section 6.2.2 (a=100 mm) was 86.2% using the raw data acquired by the network analyser and 94.1% using the post processing technique indicated by McKinzie III. Worst were the results using the large hemispherical cap (a=130 mm), 71.5% with the raw data and 92.1% using the McKinzie method.

The fact that the monopole fits tightly into the cap made impossible any study on the influence of the shifting cap centre with respect to the centre of the AUT.

2.6 First set of measurements: the Koch monopole

Four Koch monopoles, from iteration 1 to 4, were printed on a fiberglass substrate (FR4) using standard techniques for the manufacturing of printed circuits. The strips that define the intricate fractal structure have 0.35 mm width, and the thickness of the strip is 0.1 mm. Heights of the monopoles were 69.9 mm, 62.2 mm, 57.5 mm and 56.6 mm. The height of the monopoles includes a pedestal of 5 mm where the feeding pin of the SMA connector is soldered. All of them were designed to be resonant near 780 MHz, because at this frequency the compromise between manufacturing feasibility (technological limitations posed by the size of the structures) and sizes of the caps to be designed are fulfilled. Figure 10 shows the fabricated pre-fractals.

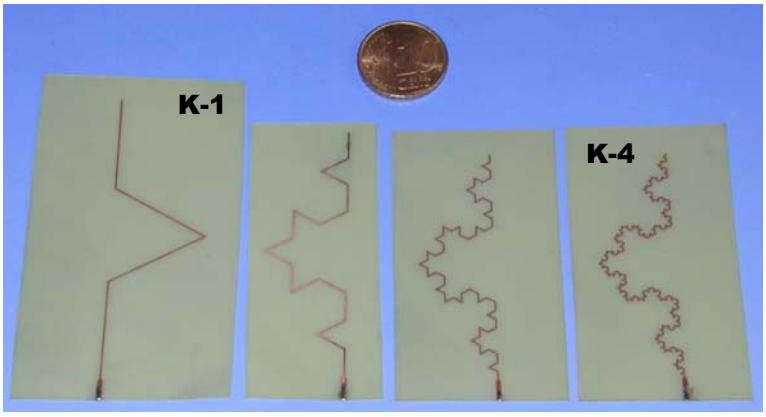

Figure 10. Pre-fractal Koch monopoles from iteration 1 to iteration 4. All are resonant at the same frequency (0.78 GHz).

A first set of measurements was carried out on the Koch monopoles using the cylindrical cap described on section 6.2.2. This cap is the one with the highest resonance and, even with the antenna closer to the walls of the shield shorter than $\lambda/2\pi$, its results agree pretty well with simulations. This fact, the distance between the walls of the radiation shield to the AUT larger than $\lambda/2\pi$, was not strictly fulfilled by other authors (for instance, [Newman, 1975]). Anyway, nowadays we are involved in the process of designing and fabricating a suitable group of caps covering the band around 0.5 – 1.5 GHz. When these caps are ready to be used a new set of data is going to be acquired and processed and more accurate results obtained for this same set of monopoles.

Previously to the measurement of the characteristic parameters (radiation efficiency and quality factor) of the Koch monopoles, they were simulated with NEC2D to predict their behaviour. Although NEC2D is not designed to analyse microstrip structures, nor is able to include dielectrics as supporting materials, their results using self-supporting wire monopoles are taken as reference. All of these limitations posed by the simulation software suppose, mainly, a shifted resonant frequency of the pre-fractals. This effect should also happen to Euclidean monopoles as a $\lambda/4$ monopole. To understand the

consequences of the limitation on the simulation software a printed $\lambda/4$ monopole, also resonant at 780 MHz, was simulated, fabricated (printed on the fiberglass substrate) and measured with the Wheeler cap method.

Table 5 resumes the simulated results for the five wired pre-fractal monopoles, showing their electrical size k_0h, efficiency η and quality factor Q. All of the parameters were simulated at resonance.

Table 6 resumes the measured results of the same parameters using the Wheeler cap method. Efficiencies and quality factors when the McKenzie post processing method is employed are also shown.

Measured efficiencies and quality factors agree qualitatively well with simulations with NEC2D. Measurements with a properly designed cap for the operating band of the antennas will improve these results, but four factors are not going to be evaluated even with that new cap: the limited size of the ground plane, the losses of the substrate, the frequency shifting effect of the substrate, and the modelling of the strips using wires (these effect is going to be cancelled using FIESTA).

Antenna	k_0h	η (%)	Q
$\lambda/4$ monopole	1.49	99.2	7.1
K-1	1.24	98.7	10.4
K-2	1.09	98.1	13.1
K-3	1.01	97.3	15.1
K-4	0.99	96.4	15.2

Table 5. Simulated electrical size k_0h, efficiency η and quality factor Q of a $\lambda/4$ monopole, and pre-fractal Koch monopoles from first to fourth iteration.

Cylindrical Cap	Wheeler method			McKinzie post processing		
Antenna	k_0h	η (%)	Q	k_0h	η (%)	Q
$\lambda/4$ monopole	1.30	92.9	7.8	1.35	92.8	5.8
K-1	1.09	89.0	12.7	1.14	90.8	8.6
K-2	0.97	86.5	16.2	1.00	88.7	13.9
K-3	0.90	83.0	18.5	0.94	86.4	13.1
K-4	0.89	82.5	18.6	0.93	86.1	13.0

Table 6. Measured electrical size k_0h, efficiency η and quality factor Q of a $\lambda/4$ monopole, and pre-fractal Koch monopoles from first to fourth iteration.

Nevertheless, measurements revealed what simulation showed: as the order of the pre-fractal increases there is a reduction on the efficiency and an increase on the quality factor. The increase in the ohmic losses of the monopole and the reduction on its radiation resistance (the increase on the slope of the input reactance of the monopole is not very remarkable) seem to be the origin of both results. Also there is evidence of

stagnation on the electrical reduction of the monopoles at self-resonance: k_0h tends to a limit value. Anyway, further research has to be carried out to confirm these preliminary results.

2.7 Conclusions

Among the methods typically used for the measurement of radiation efficiency, the Wheeler cap has been selected by its accuracy, repeatability, quick implementation, reduced measurement time, and simplicity. This selection is based not only in the referenced literature but also in experimental validation. Quality factor can also be evaluated from data get during the determination of the radiation efficiency.

Other methods, such as the Directivity/Gain in the near field, could be used to resolve doubtful results when measuring electrically small antennas.

Preliminary results on Koch monopoles using the Wheeler cap method agree with simulations about the reduction of the electrical size of the antennas with the increase on the order of the pre-fractal. Also, the radiation efficiency reduction and the quality factor increase are verified. Stagnation on all of the behaviours seems to happen. Further research is needed to confirm these results and their hypothetical causes.

2.8 References

[Andersen, 1975] Andersen, J.B.: "Antennas for VHF/UHF personal radio: a theoretical and experimental study of characteristics and performance", *IEEE Transactions on Vehicular Technology*, vol. 23, no. 4, pp. 457-461, July 1975.

[Ashkenazy, 1988] Ashkenazy, J., Levine, E., Treves, D.: "Radiometric measurement of antenna efficiency", *Electronics Letters*, vol. 21, no. 3, pp. 111 –112, 31st Jan. 1985.

[Austin, 1989] Austin, B.A.: "Resonant mode limitations with the Wheeler method of radiation efficiency measurement", *IEE Colloquium on Advances in the Direct Measurement of Antenna Radiation Characteristics in Indoor Environments*, 1989, pp. 7/1 -7/4.

[Chair, 2002] Chair, R., Luk, K.M., Lee, K.F.: "Radiation efficiency analysis on small antenna by Wheeler cap method", *Microwave and Optical Technology Letters*, vol. 33, no. 2, pp. 112 –113, April 20 2002.

[Chu, 1948] Chu, L.J.: "Physical limitations of omni-directional antennas", *Journal of Applied Physics*, vol. 19, pp. 1163-1175, 1948.

[Collin, 1964] Collin, R.E., Rothschild, S.: "Evaluation of antenna Q", *IEEE Transactions on Antennas and Propagation*, vol. 12, pp. 23-27, Jan. 1964.

[Hansen, 1981] Hansen, R.C.: "Fundamental limitations in antennas", *Proc. IEEE*, vol. 69, pp. 170-182, Feb. 1981.

[Henney, 1959] K. Henney (ed.): *Radio Engineering Handbook*, McGraw Hill, New York, 1959.

[Huang, 2001] Huang, Y., Narayanan, R.M., Kadambi, G.R.: "On Wheeler's method for efficiency measurement of small antennas", *IEEE International Symposium on Antennas and Propagation*, vol.3, pp. 346 –349, 2001.

[Ida, 1999] Ida, I., Ito, K., Okano, Y.: “Accurate measurement of small input resistances using a conventional network analyzer”, *IEEE Transactions on Antennas and Propagation*, vol. 47, no. 2, pp. 389 –391, Feb. 1999.

[Johnston, 1996] Johnston, R.H., Ager, L.P., McRory, J.G.: “A new small antenna efficiency measurement method”, *Proc. IEEE Int. Antennas and Propagat. Symp.,* 1996, vol. 1, pp. 176 –179.

[Johnston, 1998] Johnston, R.H., McRory, J.G.: “An improved small antenna radiation-efficiency measurement method”, *IEEE Antennas and Propagation Magazine*, vol. 40, no. 5, pp. 40 –48, Oct. 1998.

[Maeda, 1988] Maeda, T., Morooka, T.: “Radiation efficiency measurement method for electrically small antennas using radio wave scatterers”, *IEEE International Symposium on Antennas and Propagation*, vol. 1, pp. 324 –327, 1988.

[McKinzie III, 1997] McKinzie III, W.E.: “A modified Wheeler cap method for measuring antenna efficiency”, *IEEE International Symposium on Antennas and Propagation*, vol. 1, pp. 542 –545, 1997.

[McLean, 1996] McLean, J. S.: “A re-examination of the fundamental limits on the radiation Q of electrically small antennas “, *IEEE Transactions on Antennas and Propagation*, vol. 44, no. 5, pp. 672-676, May 1996.

[Newman, 1975] Newman, E.H., Bohley, P., Walter, C.H.: “Two methods for the measurement of antenna efficiency”, *IEEE Transactions on Antennas and Propagation*, vol. 23, no. 4, pp. 457-461, July 1975.

[Pozar, 1988] Pozar, D.M., Kaufman, B.: “Comparison of three methods for the measurement of printed antenna efficiency”, *IEEE Transactions on Antennas and Propagation*, vol. 36, no. 1, pp. 136 –139, Jan. 1988.

[Smith, 1977] Smith, G.S.: "An analysis of the Wheeler method for measuring the radiating efficiency of antennas", *IEEE Transactions on Antennas and Propagation*, vol. 25, no. 4, pp. 552-556, July 1977.

[Weiss, 2000] Weiss, S.J., Kahn, W.K.: “An experimental technique used to measure the unloaded Q of microstrip antennas”, *IEEE Transactions on Antennas and Propagation,* vol. 48, no. 1, pp. 119-122, Jan. 2000.

[Wheeler, 1959] Wheeler, H.A.: “The radiansphere around a small antenna”, *Proc. IRE*, pp. 1325 –1331, Aug. 1959.

3 GENETICALLY DESIGNED PLANAR MONOPOLES

The University of Granada applied a Genetic Algorithm optimisation technique for the design of Koch-like small antennas, developing a Pareto tool to simultaneously optimise several characteristics of planar pre-fractal wire antennas, such as efficiency, quality factor and electrical size at resonance. The code was also used to optimise intricate Euclidean structures as meander line and zigzag monopoles. The will of these computations was to assess if fractal shapes are the best alternative for the design of efficient antennas with minimum resonant frequency.

A physical constraint to the antenna dimensions was set for the three designs: the space to be filled by the antennas should not be greater than a rectangle of dimensions h x w, with h=6.22 cm and w=1.73 cm. After running the algorithm it was observed that in all the cases the optimised planar Koch-like designs offered worst radiation performances than optimised meander-line and zigzag-like designs. In few cases the pre-fractal designs reached similar characteristics than the Euclidean ones.

Figure 11 shows three examples extracted from the Pareto fronts that with the same wire length attain quite similar performances. They have been fabricated using standard photo-etching technology on a FR4 fiberglass substrate (fiberglass thickness: 0.25 mm, copper strips: 0.29 mm width and 0.25 mm thick). Once manufactured the monopoles were attached onto a 80 x 80 cm ground plane and connected to a vector network analyser through SMA connectors. The Wheeler cap method was used to evaluate the efficiency and quality factor of the monopoles at their resonant frequency. Results agreed with simulations except for the expected frequency shift and the additional losses due to the presence of the supporting substrate. Nevertheless, results confirmed the expected behaviour of the pre-fractal design.

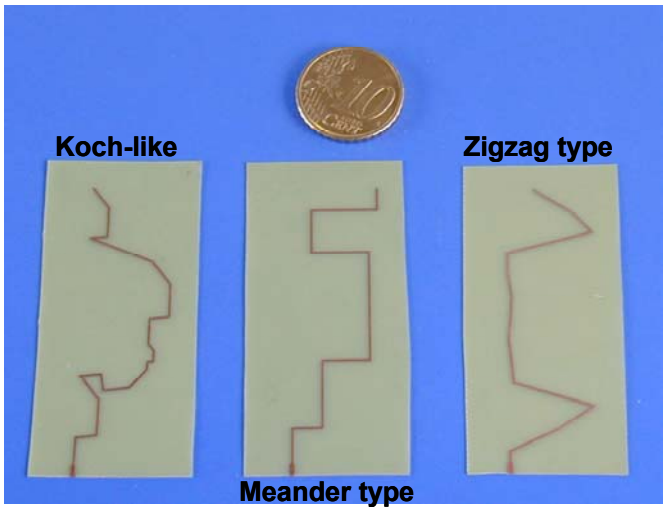

Figure 11. Genetically designed monopoles used to assess that an optimally designed self-resonant pre-fractal will perform almost as good as a Euclidean self-resonant monopole.

Tables 7 and 8 show, respectively, the computed and measured performances for these designs. The presence of a substrate was taken into account when manufacturing the monopoles and their size was scaled down according to its refraction index.

Even though, slight differences between measurements and numerical data are observed. They can be attributed to the fabrication of the antennas using strips instead of wires and also to the presence of a substrate that was not modelled by the simulator. Nevertheless, the measured data show a reasonable agreement with the numerical experiments confirming that the non-fractal antennas, either zigzag or meander, perform better than the fractal designs.

Antenna	Resonant Frequency (MHz)	Quality Factor	Efficiency (%)
Koch	864.5	13.57	96.8
Meander	826.5	12.67	97.19
Zigzag	824	13.99	96.79

Table 7. Computed performances of the genetically optimised designs.

Antenna	Resonant Frequency (MHz)	Quality Factor	Efficiency (%)
Koch	905	12.67	87.64
Meander	850	12.60	88.78
Zigzag	870	13.89	87.34

Table 8. Measured performances of the genetically optimised designs.

4 THE 3D HILBERT MONOPOLE

Three-dimensional monopoles are expected to reach lower values for the quality factor due to a more effective use of the fictitious sphere that surrounds them. Nevertheless, previous experiences with planar electrically small pre-fractals showed that both the quality factor and the efficiency values achieve worst values when increasing the fractal dimension of the monopoles. The first three iterations of a three dimensional Hilbert monopole have been designed. Their performance in terms of efficiency, quality factor, and electrical size at resonance computed and finally they have been manufactured. The radiation performance of these monopoles is ready to be measured using the Wheeler cap method.

Figures 12 and 13 show the simulated designs and their normalized current distribution along the wire. This current distribution is not much different from the sinusoidal distribution of a short dipole and reflects that in the first segments the current tends to be more uniform and that the rest of the pre-fractal behaves as a capacitive load.

Table 9 summarizes the computed parameters for these prototypes, showing that while the ratios of miniaturization are remarkable, achieved efficiencies and quality factors are

unpractical. Figure 14 shows the manufactured monopoles and their dimensions. Simulations have been carried out modelling the antennas as copper wire monopoles with 0.4 mm diameter and 89.8 mm height.

The simulations shown in this section used the well-known Method of Moments code NEC2.

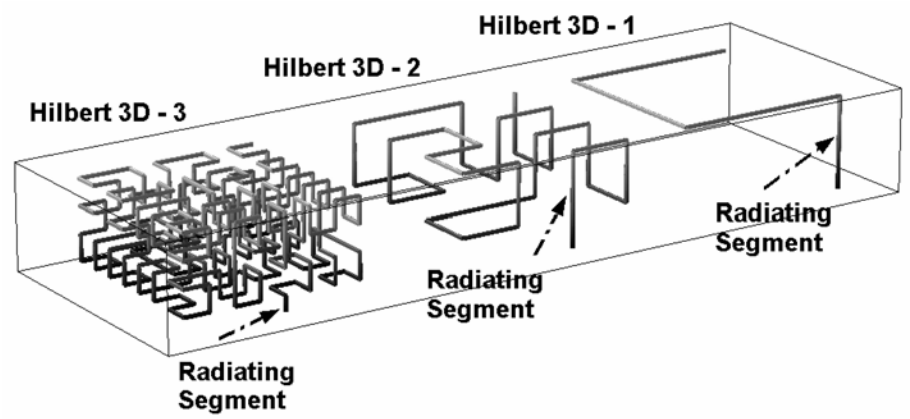

Figure 12. Simulated 3D Hilbert antennas in a monopole configuration. The first segment is the main contribution to radiation.

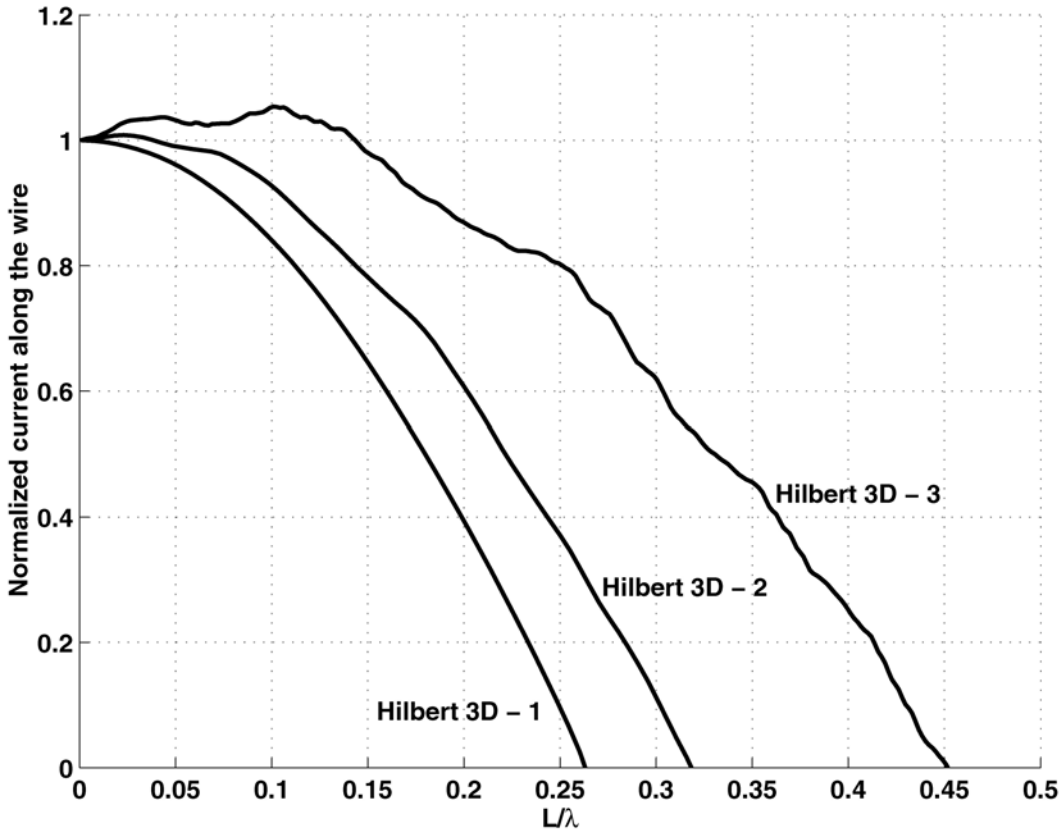

Figure 13. Normalized current distributions along the wire for the first three iterations of the 3D Hilbert monopoles.

Antenna	Total Wire Length (cm)	Electric Size at Resonance, *ka*	Resonant Frequency (MHz)	Radiation Resistance at Resonance (Ohms)	Input Resistance at Resonance (Ohms)	Efficiency (%)	Quality Factor
Hilbert 3D-1	61,78	0,71	127,5	2,47	3,24	76,6	126
Hilbert 3D-2	184,99	0,25	51,4	0,16	1,67	9,4	2091
Hilbert 3D-3	642,61	0,10	21,0	0,01	3,07	0,5	31966

Table 9. Performance of the first three iterations of a 3D Hilbert monopole.

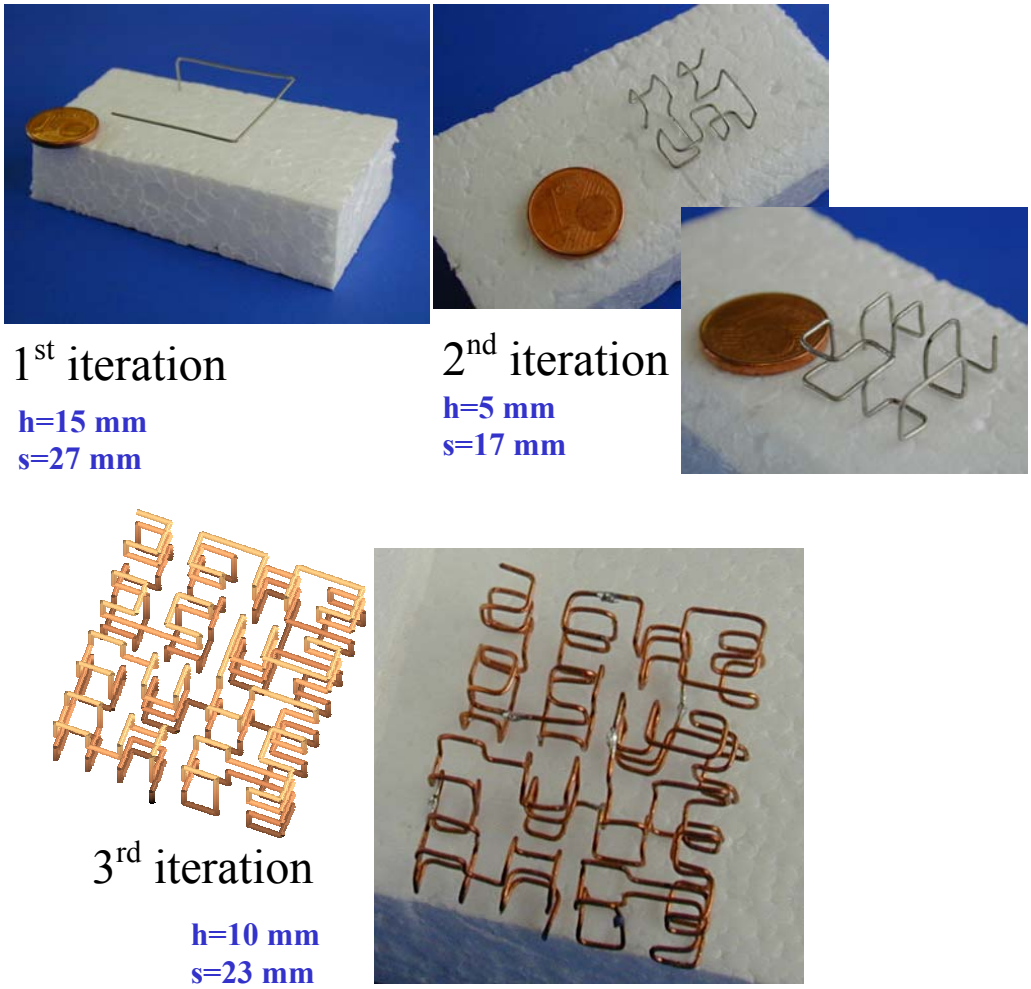

Figure 14. Fabricated 3D Hilbert monopoles. The 10 eurocents coin is used as a reference for their size.

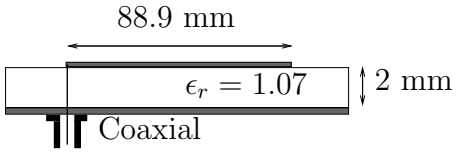

Figure 15: Profile of the Sierpinski printed antennas.

5 Prototypes and measurements at EPFL

Several prototypes of pre-fractal antennas and printed line fractal devices have been built. The kind of measurements of these devices can be separated into three groups, namely the measurements of the reflection coefficient, the measurement of the radiation characteristics (radiation pattern, efficiency), and other measurements as for example near field measurements for diagnosis purposes.

In this report three different families of microwave fractal-shaped devices are studied. The first two are based on well-known fractals, one is a surface fractal, the Sierpinski gasket, and one is a line fractal, the Koch curve. The existing literature studies the Sierpinski as a monopole [1], as well as a patch [2], [3]. In the current contribution the measurements of a Sierpinski printed antenna are presented. The Koch shaped devices studied in the existing literature are mainly based on the Koch monopole [4], but in the present report the study is done on different printed Koch-shaped structures. Finally, different line fractal shaped devices belonging to the tree family are built and measured.

6 Printed Sierpinski Gasket

6.1 Construction

The first four iterations of the Sierpinski Gasket have been built. The height of the gasket bigger triangle is h=88.9 mm.

The gaskets have been printed on a copper-berilium layer. To do so a pair of masks are needed because the photo exposition will be done on both sides of the metal. The process begins by the immersion of the cleaned metal in a photoresist bath, then the piece is put in an oven to dry the photoresist dried and adhere it to the metal. Then the piece is slided between the two masks (previously aligned in the microscope) and exposed during 140 seconds to the UV. Afterwards the metallic band exposed to the rays is put in a recipient where the developping substance is NaOH. In this way the

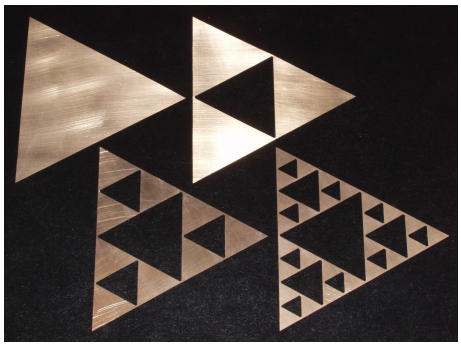

Figure 16: Copper-berilium built Sierpinski gaskets.

gasket is rendered visible, because all the parts exposed to the rays loose the deposited photoresist and only the parts covered with the mask during the UV exposition (the gasket) keep the violet characteristic color of the photoresist. The following and last step is to retire the superfluous metal by the exposition of the whole to a set of acid jets. The obtained gaskets in copper-berilium are shown in Figure 16.

To end the construction of these antennas the gaskets are going to be glued to a substrate of $\epsilon_r = 1.07$ and h=2mm and to a ground plane. The sticking process is going to be done with the help of a thin film of glue in order not to affect the permittivity of the substrate. The ground plane, the substrate, the film of glue and the gaskets are stacked and kept together with the help of two aluminum plates screwed tight, and the whole is introduced into the oven at 150°C during 45 minutes. This cooking is going to melt the glue to stick the metallic parts to the substrate.

The last step of the procedure is to solder the connector to the antenna, through a hole drilled on the ground plane and out in the vertex of the gasket. The final result is shown in Figure 17.

6.2 Measurements

6.2.1 Circuit characteristics

The reflexion coefficient for the antennas is measured in the range of 1 to 20GHz. Results are shown in Figure 18. The number of resonances diminishes as the iteration number increases, because as the subtriangles of the device become smaller for higher iterations, they resonate also at higher frequencies. In fact looking at Figure 18 we see as the magnitude of the S_{11} parameter for higher iterations seems the zoomed version of the precedent

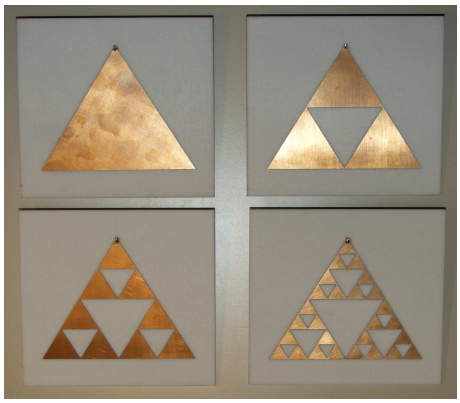

Figure 17: Printed Sierpinski antennas.

iteration, as if the curve of the response was pulled in each iteration toward the high frequencies.

6.2.2 Radiation characteristics

Radiation pattern. The radiation patterns in the E plane and the H plane are plotted for the third iteration of the Sierpinski gasket at three different frequencies. The radiation patterns are symmetric in the H plane, when the rotation axis is the axis of the connector, but they are asymmetric in the E plane, when the rotation axis is perpendicular to the connector axis. The most directive radiation pattern occurs at f=7.669GHz, Figure 19(f). At this frequency, the near field measurements (see Figure 24(c) in next section) show how the hot spots are localised in small areas and distributed in a particular way over the geometry.

Efficiency. In Table 1 we can see the different values of the antenna efficiency. Two phenomena are observed. First, the antenna efficiency diminishes for bigger iterations. Second, for a fixed iteration the efficiency is bigger at higher frequencies.

6.2.3 Near field measurements.

The method used to measure the near field of printed flat structures is based on the **modulated scatterer technique** [5]: A probe modulated at a low

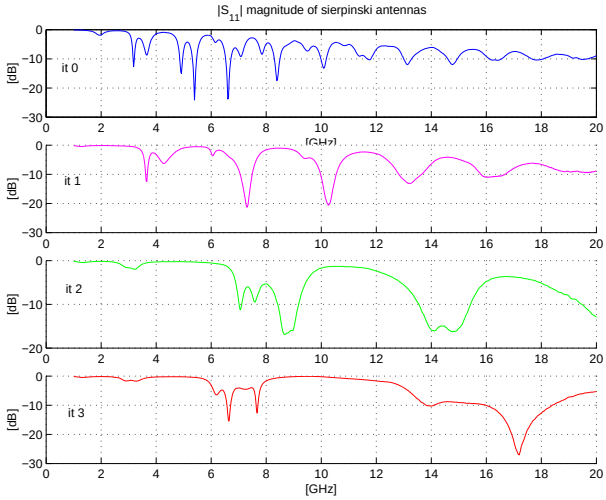

Figure 18: S_{11} magnitude for the printed Sierpinski antennas.

Antenna	Freq [GHz]	Eff [%]	Freq [GHz]	Eff [%]	Freq [GHz]	Eff [%]
it 0	5.3975	78.1	—	—	—	—
it 1	3.66	52	—	—	—	—
it 2	3.191	10.2	7.596	51.4	14.75	92.5
it 3	7.669	33.2	17.198	63.1	—	—

Table 1: Values of the measured efficiency of the Sierpinski patch iterations.

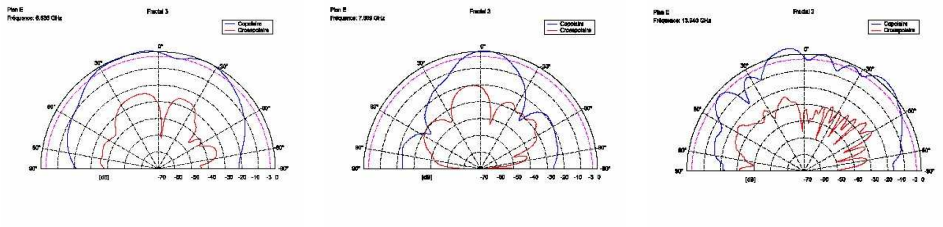

(a) E plane, f=6.635GHz (b) E plane, f=7.669GHz (c) E plane, f=13.940GHz

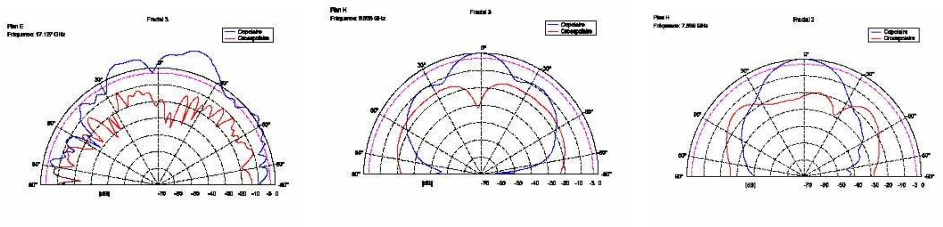

(d) E plane, f=17.127GHz (e) H plane, f=6.635GHz (f) H plane, f=7.669GHz

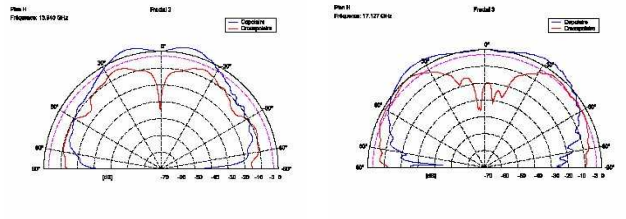

(g) H plane, f=13.940GHz (h) H plane, f=17.127GHz

Figure 19: Radiation patterns for the third iteration Sierpinski patch.

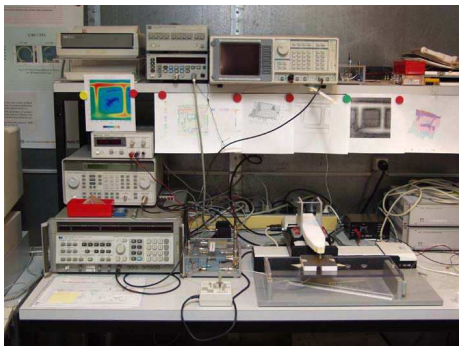

Figure 20: Near field measurement setup.

frequency by a diode perturbates locally the field component to be measured. The modulated signal comes back from the measured structure and is extracted by a homodyne receiver and a lock-in amplifier. The homodyne receivers give a high stability and sensitivity (40 to 50 dB) to the system. Both amplitude and phase of the field can be measured. The measurement setup is controlled by a computer to completely automatize the measurements. The practical interest of the presented technique is that it requires little additional investment: standard measuring equipment is used, which can be found in most microwave laboratories. No costly network analyzer is required.

Within a short period of time, it is possible to determine with a high accuracy the field distribution very close to microwave circuits and antennas, getting an excellent understanding of their physical behavior.

The measurement setup is shown in Figure 20.

The measurements for the z-component of the electric field are shown in Figure 21 for the fourth iterations of the Sierpinski printed antenna at some frequencies. The field is normalized to the maximum and covers 30dB of dynamic range (blue is -30, red is 0). For the sake of clarity the corresponding gasket has been plotted in superposition on the field measurement. The coaxial is connected in the upper vertex for all the plots. For the majority of the cases the hot spots are distributed over the metal following a clear symmetry with respect to the axis going from the excitation vertex to the base of the triangle (coinciding with the triangle height). For low frequencies the hot spots appear in the higher parts of the antenna, while for higher frequencies the hot spots are concentrated nearer to the connector. It would be very interesting to measure the near field for higher frequencies, but unfortunately for technical reasons it cannot be done for frequencies higher than 8GHz.

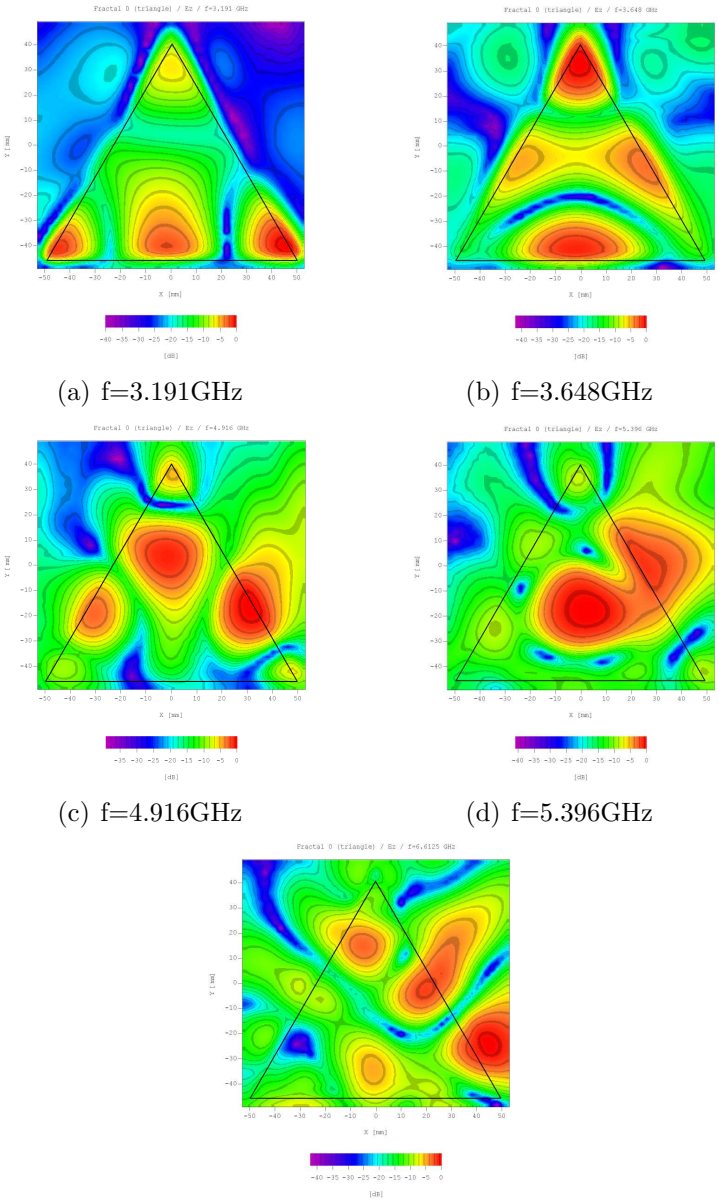

(a) f=3.191GHz

(b) f=3.648GHz

(c) f=4.916GHz

(d) f=5.396GHz

(e) f=6.6125GHz

Figure 21: Near field measurements of the iteration 0 of a printed Sierpinski antenna.

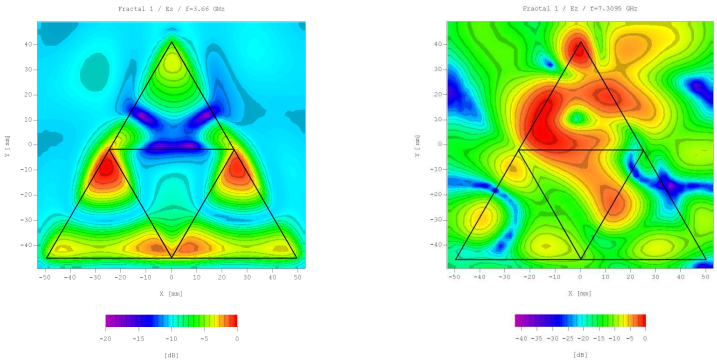

(a) f=3.66GHz (b) f=7.3095GHz

Figure 22: Near field measurements of the iteration 1 of a printed Sierpinski antenna.

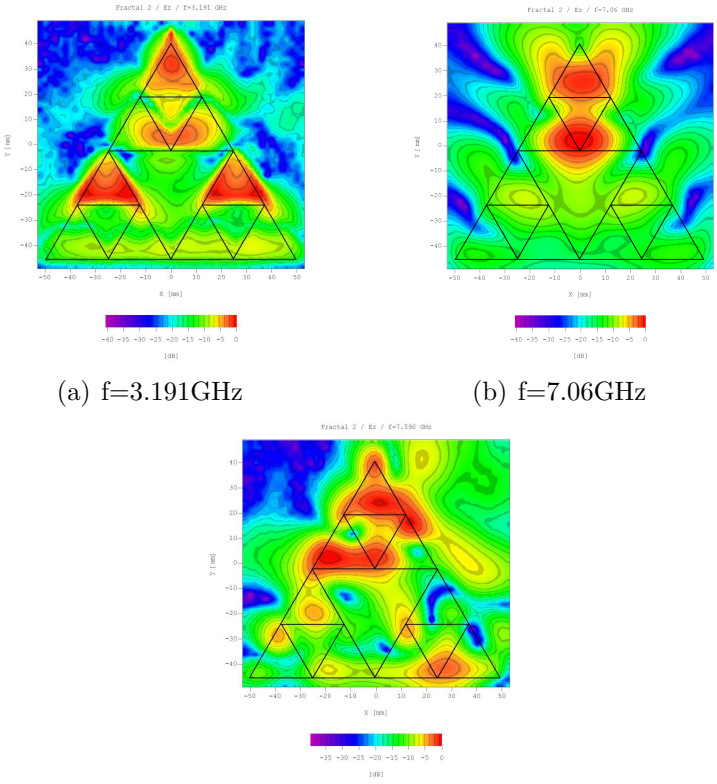

(a) f=3.191GHz (b) f=7.06GHz

(c) f=7.596GHz

Figure 23: Near field measurements of the iteration 2 of a printed Sierpinski antenna.

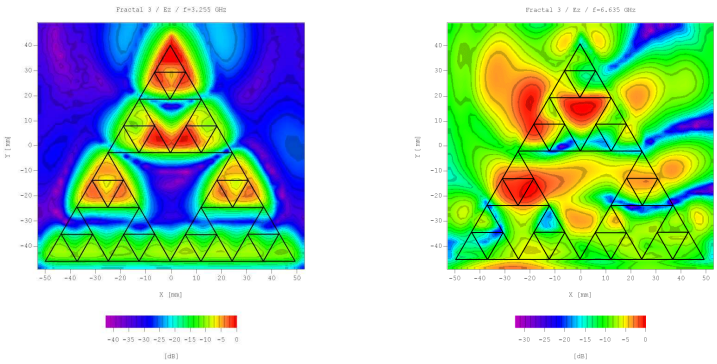

(a) f=3.191GHz (b) f=7.06GHz

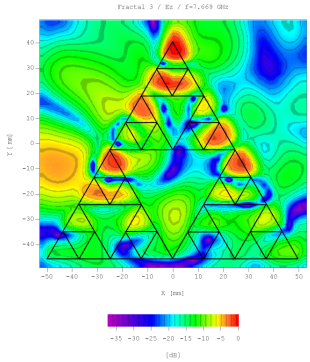

(c) f=7.596GHz

Figure 24: Near field measurements of the iteration 3 of a printed Sierpinski antenna.

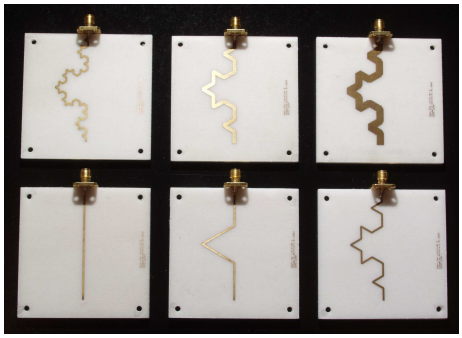

Figure 25: Printed Koch antennas.

7 Printed Koch

7.1 Construction

The antennas have been printed on epoxy of thickness 0.1 mm and following the standard procedure for printed circuits. Once the Koch lines are printed on the epoxy, a brass ground plane, a substrate $\epsilon_r = 1.07$ of 3 mm of thickness and the epoxy with the printed lines are glued together in a hot glue process, as explained for the Sierpinski antennas. In the case of the Koch antennas, 6 prototypes have been built corresponding to the iterations 0, 1, 2, 3 of the Koch, to verify the fractal properties. The antennas have been realized using a line width of w=1mm. Additionally, iteration 2 has been done also for w=2mm and w=4mm to study the influence of the line width on the antenna properties. The length of iteration 0 was l=60 mm.

7.2 Measurements

7.2.1 Circuit characteristics

In Figure 26 we can find the magnitude of the measured S_{11} parameter for the iterations 0, 1, 2 and 3 of the printed Koch for a line width of w=1 mm. Keeping the width of the line constant, different iterations are studied to see how the increment of the length of the pre-fractal affects the resonant frequency. As expected, resonances are lower for more iterated shapes. But the difference between the first resonant frequency of the iteration 1 and the iteration 2 antenna is bigger than the difference between the first resonant frequency of the iteration 2 antenna and the iteration 3 antenna (see Figure 26). This fact leads to the conclusion that at a given iteration the difference between resonance frequencies with respect to the precedent iteration will not

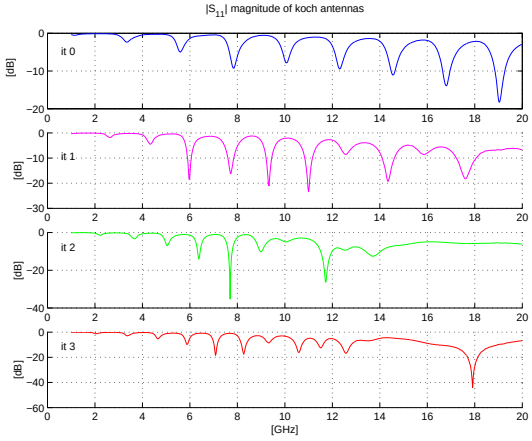

Figure 26: Reflection coefficient of the printed Koch antennas (iteration 0, 1, 2, 3) with a line width of w=1mm.

be very important, because the electric length grows in a different proportion than the physical length, the physical length grows more rapidly, as it is highlighted in Figure 27. This is due to the fact that currents do not follow the line path, which is the physical length of the structure, but they "jump" and follow a shorter path, which is proportioned by the couplings between closed segments of the lines.

Next, a comparison between the resulting printed Koch antennas in the second iteration but with different line width is done. The reason for choosing the second iteration is the limitation encountered when iterating with a thick line. When the line is thick for a high iteration the Koch does not keep the proportions, and looses the Koch shape.

In Figure 28 the magnitude of the measured S_{11} parameter for the iteration 2 is shown for three different line widths (1mm, 2mm, 4mm). The observed effect is that for a fixed iteration (that is the same as saying for the same electrical length) the resonance frequency becomes higher when the line is thicker.

7.2.2 Radiation characteristics

Radiation pattern. The radiation patterns in the E and H planes have been measured. The E plane is the plane where the antenna under test turns in the axis perpendicular to its main axis, and the H plane is the plane where the antenna rotates on its main axis. In Figure 29 the setup of the measurement in the H plane can be seen.

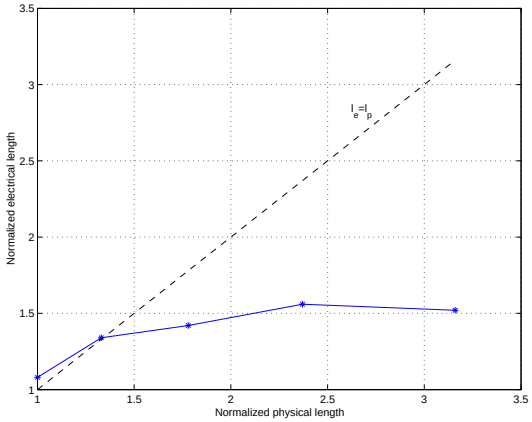

Figure 27: Normalized electrical length as a function of the normalized physical length (solid line). The curve $l_e = l_p$ is plotted in dashed line for comparison.

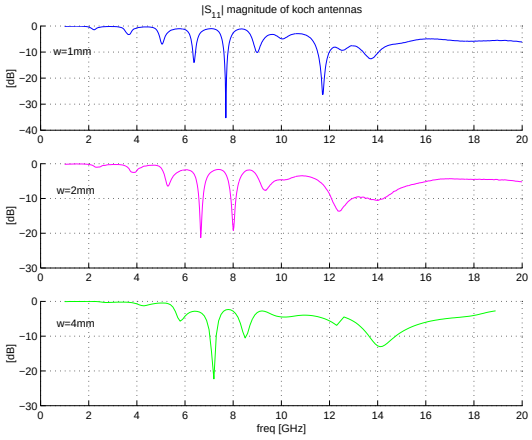

Figure 28: Reflection coefficient of the printed Koch antennas (iteration 2) for three different line widths: w=1mm, 2mm and 4mm.

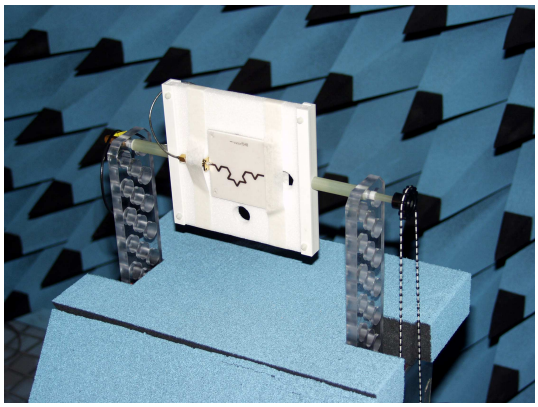

Figure 29: Measurement of the radiation in the H plane.

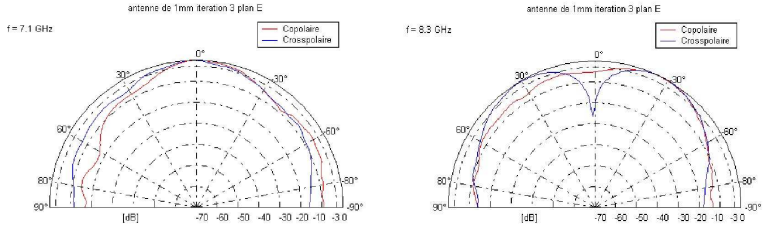

(a) E plane, f=7.1GHz (b) E plane, f=8.3GHz

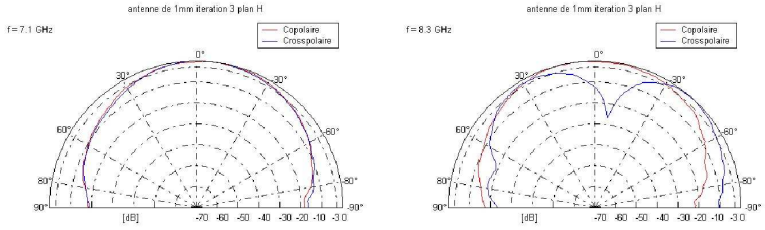

(c) H plane, f=7.1GHz (d) H plane, f=8.3GHz

Figure 30: Radiation patterns for the third iteration of the printed Koch.

Antenna	Frequency [GHz]	Efficiency [%]
it 1, w=1mm	9.33	44.20
it 2, w=1mm	7.7	45.10
it 3, w=1mm	7.1	52
it 2, w=2mm	6.65	53.20
it 2, w=4mm	7.03	61.40

Table 2: Values of the measured efficiency of the printed Koch different iterations.

In Figure 30 some of the measured radiation patterns for the third iteration Koch with a line width of 1mm are shown. In general we find a typical dipole pattern. All the patterns are symmetric except the measurements in the H plane at 8.3GHz.

Efficiency. In Table 2 the values of the efficiency measured at the different resonances of the Koch antennas are shown. The efficiency has been measured for the different iterations and also for the different line widths. Two phenomena are observed. First, the efficiency increases with the iteration. This is due to the fact that increasing the iteration the number of bendings increases, and the more discontinuities there are, the more radiation there is. Second, for the same iteration, the efficiency is higher for wider lines, because, obviously, when the line is wider the emitting surface is bigger.

7.2.3 Near field measurements.

The near field measurements of the second iteration of the printed Koch antenna with a line width of w=4 mm has been done for the frequency f=7.03GHz. The measurements can be seen in Figure 31, where a shadow of the Koch-shaped antenna has been superposed for the sake of clarity. It can be observed that the hot spots and the cold spots are separated by a distance of 4 mm, which is the value of λ for this frequency.

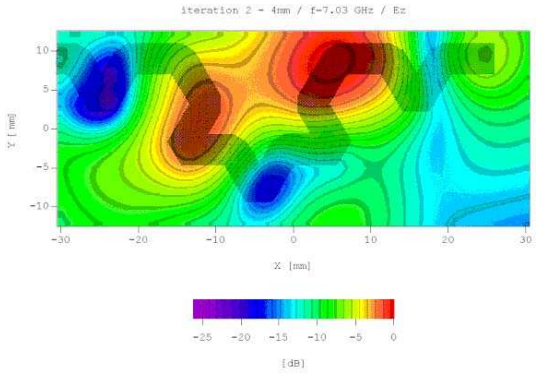

Figure 31: Near field measurement of the second iteration printed Koch antenna.

8 Printed fractal-shaped line devices

Some prototypes of two-port structures belonging to the tree family [6] have been built and measured.

8.1 Construction

All the prototypes have been printed on a layer of epoxy 0.1mm and hot glued to a 1mm thick foam, of $\epsilon_r = 1.07$ and the whole over a ground plane. In Figure 32 the top views of the built prototypes are shown.

In order to avoid the imperfections in the transition between the connector and the lines, the soldering of the connectors is avoided by the use of the test fixture shown in Figure 33. It consists of 4 coaxial connectors, that can be moved on a guide, or moved translationarilly by changing the position of the platform they are on.

To improve the quality of the measurement a TRL (trough reflection line) calibration has been done. In this way the effect of the transition between the connector and the line is taken into account and compensated.

8.2 Measurements

8.2.1 Characteristics of the circuit

In Figure 34 the measured scattering parameters of a two order square capillar are compared to those obtained with our transmission line model and a fullwave commercial software. The first thing to comment is that the global shape of the three graphics is mostly similar, except for the losses observed

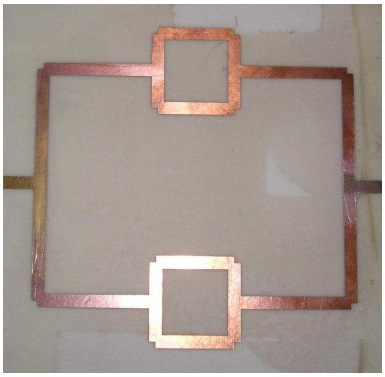

(a) Order 2 square.

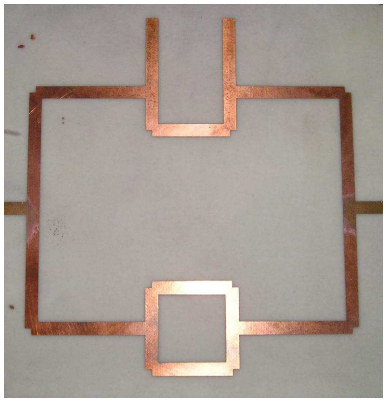

(b) Order 2 square with different seed.

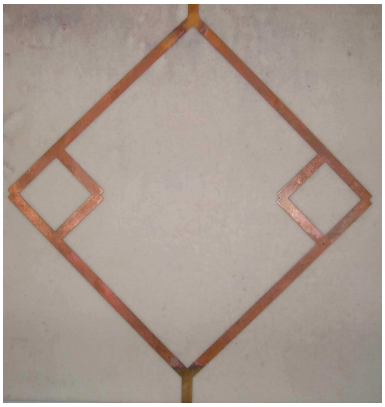

(c) Order 2 rhomb.

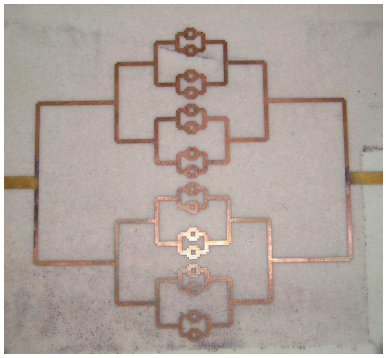

(d) Order 5 square.

Figure 32: Prototypes.

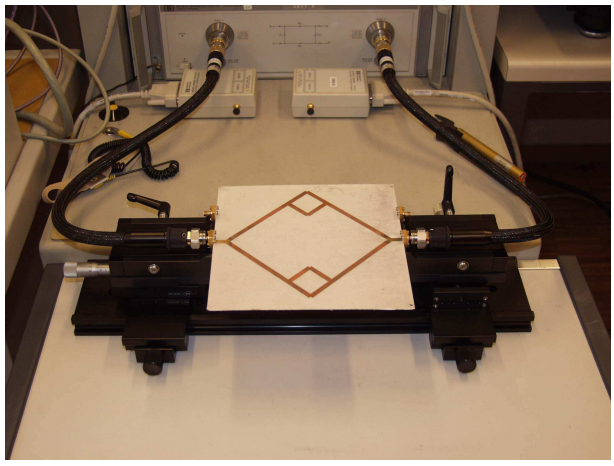

Figure 33: Measurement of one of the prototypes.

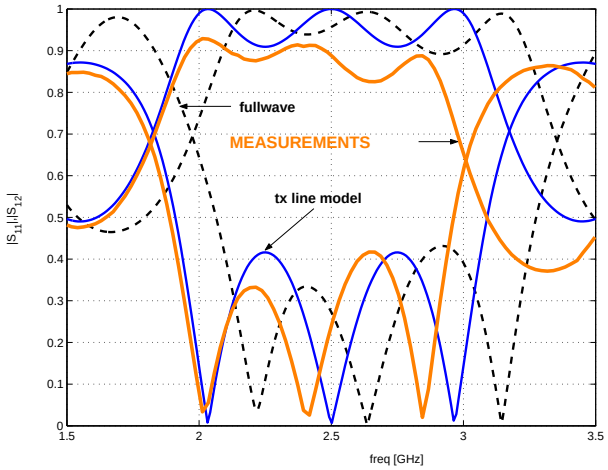

Figure 34: Comparison of the magnitude of S_{11} and S_{21} for a two order square capillar (transmission line model, fullwave model and measurements).

in the measurements and not appearing in the two models, because losses are not taken into account during the simulations. When comparing transmission line model to the fullwave model, the most significant difference between the two models was a shift in frequency: the fullwave model had a mismatching toward the higher frequencies with respect to the transmission line model. It was expected for measurements to be nearer to the fullwave model than to the transmission line model. Unexpectedly, it turns out to be the contrary, the transmission line model gives a response more approximated to the measured frequencies. Particularly good is the matching at the lower resonance frequency, where the transmission line model coincides with the measurement, whereas the fullwave model gives a lousy prediction of the measurements. For higher frequencies there is a shift appearing for both models with respect to the measurements, but the shift is always smaller for the transmission line model. Concerning the ripple it must be mentioned that the fullwave model predicts better the level of the ripple than the transmission line model, surely because of the coupling between the lines, that is completely neglected in the transmission line model.

In Figure 35 the measured scattering parameters of a two order rhomb capillar are compared to those obtained with the transmission line model and the fullwave commercial software. Contrarily to the square case, the global shape is changing from one model to another and also from measurements to the models. The spike appearing in the fullwave model analysis appears also in the measurements, although less emphasized in the measurements. The

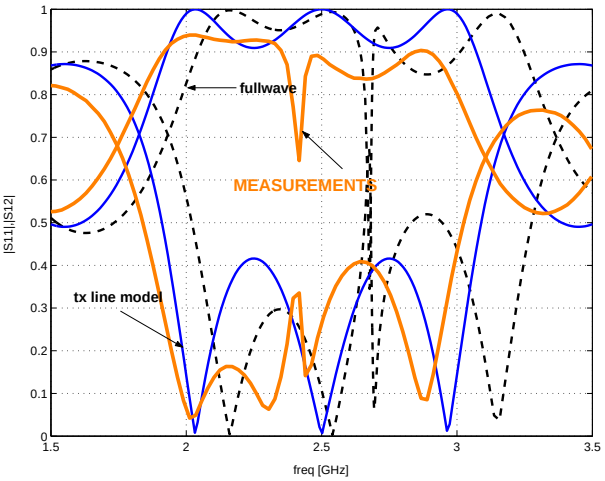

Figure 35: Comparison of the magnitude of S_{11} and S_{21} for a two order rhomb capillar (transmission line model, fullwave model and measurements).

spike is probably due to the couplings existing for this topology of capillar and not for a square one. Again as in the square case the transmission line model gives a better approximation to the measurements for low frequencies than the fullwave model but there is a frequency shift appearing, that, however, is more important for the fullwave model.

In Figure 36 the measured scattering parameters of a two order square capillar with a open circuit as the seed of one of its branches are compared to those obtained with the transmission line model and the fullwave commercial software. The spike predicted with the fullwave software is also appearing in the measurements, but less strong. For this structure neither transmission line model nor fullwave model are giving a reasonable prediction of the measured response, there is a frequency shift for all the frequencies, although again it is smaller for the transmission line model. Nevertheless, the models are more similar to each other than to the measurements.

9 Conclusions and future work at EPFL

Different printed fractal-shaped devices have been built and measured. The devices have been characterized in terms of reflection coefficient, radiation properties and near field measurements.

The reflection coefficient of the Sierpinski patch antenna has shown a multiband behavior of the device. With the near field measurements the

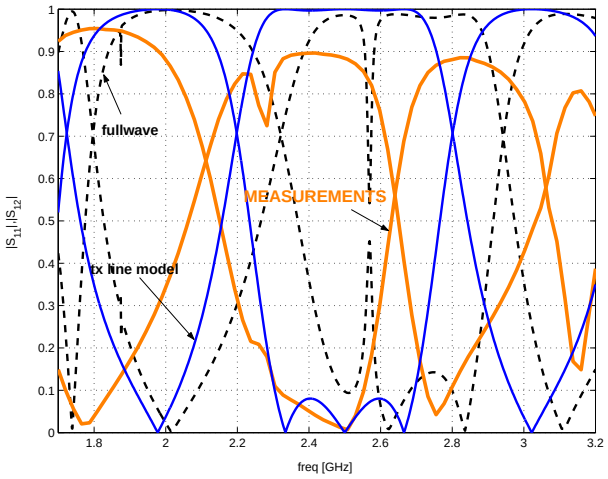

Figure 36: Comparison of the magnitude of S_{11} and S_{21} for a two order square capillar with different seed (transmission line model, fullwave model and measurements).

distribution of hot spots has been studied, as well as the radiation properties produced by the field distribution. The efficiency measurements have shown that the efficiency diminishes with the iteration but grows with the frequency.

The reflection coefficient of the printed Koch line has shown the relation of the resonant frequency with the iteration of the fractal shape and with the width of the line. First, the resonant frequency diminishes when the iteration increases, until a certain limit. Then, for the same iteration the resonant frequency is higher if the line is thicker. In terms of the efficiency it can be said that the higher the iteration, the higher the efficiency, and the thicker the line is, the higher the efficiency is as well.

The measured reflection coefficient of the capillar fractal shows good agreement with the developed transmission line model, but the levels of the ripple and the slopes of the response in the bands of interest have to be ameliorated.

References

[1] C. Puente-Baliarda, J. Romeu, R. Pous, A. Cardama: *On the Behavior of the Sierpinski Multiband Fractal Antenna*, IEEE Transactions on Antennas and Propagation, Vol. 46, No. 4, April 1998.

[2] J. Parrón, J.M. Rius, J. Romeu: *Analysis of a Sierpinski fractal patch antenna using the concept of macro basis functions*,IEEE Antennas and Propagation Society International Symposium 2001, Vol. 3 , 8-13 July 2001.

[3] C. Borja, J. Romeu: *Multiband Sierpinski Fractal Patch Antenna*, IEEE Antennas and Propagation Society International Symposium, 2000. Vol. 3, 16-21 July 2000.

[4] C. Puente-Baliarda, J. Romeu, A. Cardama *The Koch Monopole: A Small Fractal Antenna*, IEEE Transactions on Antennas and Propagation, Vol. 48, No. 11, November 2000.

[5] J.F. Zürcher:*High performance near field measurements for antennas and microstrip circuits*, Precision Electromagnetic Measurements, 1994. Digest., 1994 Conference on , 27 June-1 July 1994.

[6] E. Cabot, J.R. Mosig: *Analysis methods for fractal-shaped printed line devices*, 27th ESA Antenna Technology Workshop on Innovative Antennas, 9-11 March 2004. Accepted for publication.

DISCLAIMER

The work associated with this report has been carried out in accordance with the highest technical standards and the FRACTALCOMS partners have endeavoured to achieve the degree of accuracy and reliability appropriate to the work in question. However since the partners have no control over the use to which the information contained within the report is to be put by any other party, any other such party shall be deemed to have satisfied itself as to the suitability and reliability of the information in relation to any particular use, purpose or application.

Under no circumstances will any of the partners, their servants, employees or agents accept any liability whatsoever arising out of any error or inaccuracy contained in this report (or any further consolidation, summary, publication or dissemination of the information contained within this report) and/or the connected work and disclaim all liability for any loss, damage, expenses, claims or infringement of third party rights.